Climatic and palaeoceanographic changes during the Pliensbachian (Early Jurassic) inferred from clay mineralogy and stable isotope (C-O) geochemistry (NW Europe)

Accepted 09/01/17 Global and Planetary Change

Cédric Bougeault [a], Pierre Pellenard [a], Jean-François Deconinck [a], Stephen P. Hesselbo [b], Jean-Louis Dommergues [a], Ludovic Bruneau [a], Théophile Cocquerez [a], Rémi Laffont [a], Emilia Huret [c], Nicolas Thibault [d]

[a] UMR CNRS 6282 Biogéosciences, Univ. Bourgogne Franche-Comté, 6 Boulevard Gabriel, 21000 Dijon, France

[b] Camborne School of Mines, and Environment and Sustainability Institute, University of Exeter, Penryn Campus, Penryn, TR10 9EZ, UK

[c] ANDRA, Parc de la Croix-Blanche, 1-7 rue Jean Monnet, 92298 Châtenay-Malabry, France

[d] Department of Geosciences and Natural Resource Management, University of Copenhagen, Øster Voldgade 10, DK-1350 Københavns K., Denmark

Corresponding author: C. Bougeault (cedricbou@orange.fr)

Abstract

The Early Jurassic was broadly a greenhouse climate period that was punctuated by short warm and cold climatic events, positive and negative excursions of carbon isotopes, and episodes of enhanced organic matter burial. Clay minerals from Pliensbachian sediments recovered from two boreholes in the Paris Basin, are used here as proxies of detrital supplies, runoff conditions, and palaeoceanographic changes. The combined use of these minerals with stable isotope data

(C-O) from bulk carbonates and organic matter allows palaeoclimatic reconstructions to be refined for the Pliensbachian. Kaolinite/illite ratio is discussed as a reliable proxy of the hydrological cycle and runoff from landmasses. Three periods of enhanced runoff are recognised within the Pliensbachian. The first one at the Sinemurian-Pliensbachian transition shows a significant increase of kaolinite concomitant with the negative carbon isotope excursion at the so-called Sinemurian Pliensbachian Boundary Event (SPBE). The Early/Late Pliensbachian transition was also characterised by more humid conditions. This warm interval is associated with a major change in oceanic circulation during the Davoei Zone, likely triggered by sea-level rise; the newly created palaeogeography, notably the flooding of the London-Brabant Massif, allowed boreal detrital supplies, including kaolinite and chlorite, to be exported to the Paris Basin. The last event of enhanced runoff occurred during the late Pliensbachian (Subdonosus Subzone of the Margaritatus Zone), which occurred also during a warm period, favouring organic matter production and preservation. Our study highlights the major role of the London Brabant Massif in influencing oceanic circulation of the NW European area, as a topographic barrier (emerged lands) during periods of lowstand sea-level and its flooding during period of high sea-level. This massif was the unique source of smectite in the Paris Basin. Two episodes of smectite-rich sedimentation (‘smectite events’), coincide with regressive intervals, indicating emersion of the London Brabant Massif and thus suggesting that an amplitude of sea-level change high enough to be linked to glacio-eustasy. This mechanism is consistent with sedimentological and geochemical evidences of continental ice growth notably during the Latest Pliensbachian (Spinatum Zone), and possibly during the Early Pliensbachian (late Jamesoni/early Ibex Zones).

Keywords

Early Jurassic, Pliensbachian, runoff, clay minerals, stable isotope, glacio-eustasy

1. Introduction

The Early Jurassic was a period of major environmental and biological changes contemporaneous with the break-up of Pangaea and intense volcanic phases linked to the CAMP (Central Atlantic Magmatic Province) and the Karoo-Ferrar large igneous provinces (Little and Benton, 1995; Wignall, 2001; Wignall et al., 2005; Jourdan et al., 2008; Schaltegger et al., 2008; Dera et al., 2011a; Guex et al., 2016). During the Early Toarcian, prominent organic matter (OM) accumulations in marine sediments, associated with anoxic conditions, were recorded in many parts of the world, defining the well-known and extensively studied Toarcian Oceanic Anoxic Event (T-OAE). A remarkable positive shift of the $\delta^{13}C$ values was triggered by OM storage in oceanic sediments (Jenkyns, 1988, 2010; Al-Suwaidi et al., 2010; Suan et al., 2011; Izumi et al., 2012; Krencker et al., 2014). Within this positive carbon isotope excursion a strong negative carbon isotopic excursion (CIE) of -7‰ in average amplitude has been recognised in terrestrial organic matter and in marine sediments (Hesselbo et al., 2000a; Schouten et al., 2000; Kemp et al., 2005; van de Schootbrugge et al., 2005; Hesselbo et al., 2007; Hesselbo and Pieńkowski, 2011). Intense volcanic activity from the Karoo-Ferrar magmatic province coupled with an increase of runoff conditions and temperature triggering oceanic methane injection and consequently light carbon release is a prominent suggestion to explain this negative excursion (Hesselbo et al., 2000a; Hesselbo et al., 2007; Suan et al., 2011; Hermoso and Pellenard, 2014). New data from the Pliensbachian interval show that two other excursions in the $\delta^{13}C$ biogenic carbonate and organic matter content occurred: 1) a negative excursion (-2‰) at the Sinemurian-Pliensbachian boundary, namely the Sinemurian-Pliensbachian Boundary Event (SPBE) 2) a positive excursion (+2‰) during the Late Pliensbachian corresponding to the Late Pliensbachian Event (Korte and Hesselbo, 2011; Silva et al., 2011; Franceschi et al., 2014; Silva and Duarte, 2015; Gómez et al., 2016; Peti et al., submitted). Most of these events are coeval with variations of seawater temperatures calculated

from $\delta^{18}O$ values of bulk carbonate and calcified organisms. Warm periods occurred during the Late Sinemurian and the Early-Late Pliensbachian transition (e.g. Ibex to early Margaritatus Zones; Korte and Hesselbo, 2011; Silva and Duarte, 2015; Martinez and Dera, 2015; Gómez et al., 2016), while a cooler phase was recognised during the Late Pliensbachian mainly on the basis of $\delta^{18}O$ data measured from belemnite rostra (Rosales et al., 2004; Dera et al., 2009b; Korte and Hesselbo, 2011; Martinez and Dera, 2015; Gómez et al., 2016), brachiopods and bivalves shells (Suan et al., 2010; Korte and Hesselbo, 2011) and from sedimentological and palynological evidences (Price, 1999; Suan et al., 2011). Together with available $\delta^{13}C$ and $\delta^{18}O$ data, clay minerals could be used as an informative palaeoclimatic proxy, especially to better constrain continental weathering and humidity/aridity variations (Robert and Kennett, 1994; Vanderaveroet et al., 1999; Ruffell et al., 2002; Pellenard et al., 2014). The kaolinite/illite ratio is considered to be a reliable proxy of humid conditions during the Jurassic (Chamley, 1989; Hallam et al., 1991; Pellenard and Deconinck, 2006; Raucsik and Varga, 2008; Dera et al., 2009a; Hesselbo et al., 2009; Hermoso and Pellenard, 2014; Pellenard et al., 2014). Kaolinite contents have been used to build long-term palaeohumidity curves for the Pliensbachian-Toarcian interval (Dera et al., 2009a). At the scale of the Tethyan domain, global enrichments of kaolinite during the Davoei Zone and during the early Toarcian (Falciferum to Bifrons Zones) were interpreted as periods of enhanced runoff on landmasses, while decreasing proportions of this mineral during the late Pliensbachian, suggested a colder and drier period, in agreement with the $\delta^{18}O$ fluctuations (Dera et al., 2009a, 2009b, 2011a; Martinez and Dera 2015; Gómez et al., 2016). In more detail, a significant and brief increase of kaolinite was also identified at the base of the Serpentinum Zone, synchronous with the negative shifts in carbon isotopes ($\delta^{13}C_{org}$ and $\delta^{13}C_{carb}$), and associated with an increase of temperature measured from the $\delta^{18}O$ bulk carbonate (Hermoso and Pellenard, 2014). Again, the enrichment of kaolinite

97 supports enhanced runoff and continental weathering during a brief warming episode and the
98 reliability of clay minerals as sensitive climate proxies.

99 Despite these relationships between clay mineralogy and geochemical proxies in the late
100 Pliensbachian and Toarcian, links between $\delta^{13}C$ disruption, sea temperature change, and
101 kaolinite enrichment still remain poorly described in the remaining Lower Jurassic. In the
102 present study, we cover the entire Pliensbachian stage through a high-resolution analysis of clay
103 mineralogy and carbon and oxygen isotopes in multiple sections from the NW European
104 domain well-constrained by ammonites and/or calcareous nannofossils. Relationships between
105 clay mineralogy, $\delta^{13}C$ excursions, and $\delta^{18}O$ fluctuations are carefully examined in order to
106 decipher the role of the carbon cycle and temperature evolution on continental weathering
107 changes. Palaeoceanographic changes, eustatic variations, and detrital sources, are also
108 discussed in relation to palaeoclimate changes.

109

110 ## 2. Geological setting

111 During the Early Jurassic, the NW Tethyan domain corresponded to the extension of the
112 Tethys Ocean which was characterised by an archipelago, composed of large islands inherited
113 from the Variscan orogeny surrounded by epicontinental seas (Thierry et al., 2000). The NW
114 Tethyan domain was also connected to the Arctic Sea and the Panthalassa Ocean through the
115 Viking and Hispanic corridors implying different water mass influences (Dera et al., 2009b).
116 This domain is generally subdivided into two parts, with the Mediterranean area, and a NW
117 European domain that includes the Paris and the Wessex basins where boreholes and sections
118 analysed in this study are located (Fig. 1).

119 The Paris Basin is an intracratonic basin surrounded by four landmasses, namely the
120 London-Brabant Massif to the north, the Armorican Massif to the west, the Central Massif to

121 the south and the Bohemian Massif to the east. Located in the southern part of the Paris Basin,
122 to the north of the Central Massif, the Sancerre borehole (Callovian to Carboniferous) was
123 drilled during the “Géologie Profonde de la France” programme (Deep Geology of France,
124 Lorenz et al., 1987). From the end of the Sinemurian to the Lower Pliensbachian, sediments are
125 dominantly clayey limestone, while the Upper Pliensbachian is marked by claystone. The
126 Pliensbachian-Toarcian boundary is characterised by some limestone beds. The Lower
127 Toarcian strata comprise marl and organic-rich shale beds. Previous mineralogical and
128 geochemical investigations were performed by Delavenna et al. (1989), Hermoso et al. (2009,
129 2012, 2013) and Hermoso and Pellenard (2014). From this core, 283 samples were analysed by
130 X-ray diffraction.

131 The Montcornet borehole (A901 site) is located close to the Ardennes Massif in the
132 northern part of the Paris Basin. Reaching 1100 metres in depth, it was drilled by Andra (the
133 French National Radioactive Waste Management Agency) from Turonian chalks to the
134 Devonian basement. The Lower Pliensbachian is composed of marl and limestone beds with
135 pyritised burrows and phosphate nodules in the upper part. The Upper Pliensbachian comprises
136 marl and claystone with some diagenetic siderite-rich nodules and thin accumulations of bivalve
137 shells interpreted as tempestites. The Pliensbachian-Toarcian boundary is poorly defined
138 biostratigraphically, but likely corresponds to the occurrence of limestone beds, coeval with the
139 "Grès Médioliasiques" Fm, recognised in the rest of the Paris Basin and interpreted as a
140 regressive facies (Brigaud et al., 2014). The Toarcian is characterised by locally organic-rich
141 and laminated shale. An abundant fauna including nektonic (ammonites and belemnites) and
142 benthic organisms (bivalves, brachiopods, crinoids) occurs throughout the core. Previous
143 analyses have been performed on biostratigraphy, magnetostratigraphy (Yang et al., 1996;
144 Moreau et al., 2002) and mineralogy (Debrabant et al., 1992). 197 samples have been analysed

for clay mineralogy and 213 samples for isotope geochemistry. In addition, 50 new specimens of ammonites have been collected to help refine the biostratigraphy.

Additional clay mineral data from two sections (Corbigny, South Paris Basin, France and Charmouth, Wessex Basin, U.K) have been used for further comparisons (Fig. 1).

3. Materials and methods

3.1. Clay mineralogy

A total of 480 samples have been analysed using X-Ray Diffraction (XRD). After a gentle crush, powdered samples were decarbonated with a 0.2M HCl solution. The fraction below two microns (clay sized particles), was extracted with a syringe after decantation of the suspension during 1h35 following the Stokes law, and then centrifuged. Ammonia water was added to samples from Sancerre to help their deflocculation as recommended by Holtzapffel (1985). Clay residue was then smeared on oriented glass slides and run in a Brucker D4 Endeavour diffractometer with CuKα radiations, LynxEye detector and Ni filter under 40 kV voltage and 25 mA intensity (Biogeosciences laboratory, University of Burgundy). Scanning from the goniometer ranges from 2.5° to 28° for each analysis. Three runs were performed for each sample to discriminate clay phases: 1) Air-drying; 2) Ethylene-glycol solvation; 3) Heating at 490°C, as recommended by Moore and Reynolds (1997). Clay minerals were identified using their main diffraction (d_{001}) peak and by comparing the three diffractograms obtained. Clay minerals identified are the following: R0 type illite-smectite mixed-layer (17 Å based on glycolated run condition) referred to smectite for the following sections; R1 type illite-smectite mixed-layer (around 11.5 Å on air-drying conditions and 13 Å after ethylene-glycol solvation); chlorite (14.2 Å, 7.1 Å, 4.7 Å and 3.54 Å peaks); illite (10 Å, 5 Å, 3.33 Å); kaolinite (7.18 Å and 3.58 Å peaks). Estimated proportions of each clay mineral were performed using the

MacDiff 4.2.5 software (Petschick, 2000) on glycolated diffractograms. As the main (d_{001}) peak of kaolinite and the (d_{002}) peak of chlorite are overlapping, a deconvolution procedure was applied on the (d_{004}) peak area of chlorite (3.54 Å) and (d_{002}) peak area of kaolinite (3.57 Å) to estimate properly both minerals proportions using the 7.1 peak ($d_{001kaolinite} + d_{002chlorite}$). Chlorite percentage was calculated using the mean between (d_{001}) and (d_{002}) chlorite peak areas considering that chemical nature in chlorite impact the (d_{001})/(d_{002}) ratio (Moore and Reynolds, 1997). The K/I ratio based on (d_{001}) peak area of each minerals was systematically calculated. Scanning Electronic Microscope (SEM) observations were performed with a JEOL JSM 6400F Field Emission SEM (ARCEN platform of the LICB laboratory of the University of Burgundy).

3.2. Geochemical analyses

Isotope analyses on bulk carbonate oxygen and carbon ($\delta^{18}O_{Carb}$ and $\delta^{13}C_{Carb}$) were performed using a carbonate preparation device Kiel IV coupled with a Delta V Plus mass spectrometer (ThermoFisher) at the Biogeosciences laboratory (University of Burgundy). 130-900µg of rock were cleaned with ethanol, finely powdered and dried at 50°C for 12 hours in a stove. Carbonates were reacted with purified orthophosphoric acid at 70°C. Samples were calibrated to V-PDB using NBS-19. Replicates were regularly made to evaluate reproducibility which are respectively of 0.04‰ and 0.08‰ for $\delta^{13}C_{Carb}$ and $\delta^{18}O_{Carb}$.

3.3. Statistical analyses

The SiZer analysis (Significance of Zero crossings of smoothed estimates e.g. Marron and Chaudhuri, 1998) was used on the K/I ratio to define significant changes in kaolinite content. This method consists on the analysis of the derivative of a smoothed curve obtained from a kernel type regression using different levels of smoothing (noted *h*). SiZer method compiles derivative curves with their 95% confidence intervals. The morphology of the curves is analysed on the second derivative to identify wide patterns (bulge, hollow) and short patterns

193 (peak) suggested from the biostratigraphic framework. Results are presented on a SiZer map
194 indicating significant changes in the curve morphology of the investigated parameter. The
195 abscissa characterises the level of smoothing (window size *h* in log scale) and the ordinate the
196 depth. Long amplitude changes in the K/I ratio are detected on large window analysis (*i.e.* h =
197 log (1)), whereas short amplitude changes are detected on short window analysis (*i.e.* h = log
198 (0)). Bulges are shown in red, hollows in blue. Grey surfaces are interpreted as not statistically
199 significant.

200

201 ## 4. Results

202 ### 4.1 Biostratigraphic framework

203 The biostratigraphic framework has been recently revised at Sancerre (see Peti et al., in
204 press). At Montcornet, new investigations have been conducted to complete the study of
205 Moreau et al., (2002). All ammonites chronozones are recognised in the Pliensbachian stage
206 except the Spinatum Zone. Ammonites and biozonation boundaries are precisely reported on
207 Fig. 2 and synthetically reported on Figs. 3 and 4 (grey intervals are considered as intervals of
208 uncertainties). The detail of identified ammonites and their biostratigraphic attribution are
209 reported in the supplementary file (Suppl. Mat. Fig. 1).

210

211 ### 4.2 Clay mineralogy

212 #### *4.2.1. Sancerre borehole (South Paris Basin)*

213 Clay mineral assemblages from the Sancerre borehole mainly comprise kaolinite (13-
214 50%), illite (24-57%), R1 Type illite-smectite mixed-layer (IS R1; 13-29%) and chlorite (7-
215 24%; Fig. 3). The main features are coeval variations between: 1) kaolinite and chlorite, and;

2) illite and IS R1. As a consequence, kaolinite and illite contents are inversely related, and these minerals also display the greatest variations, which exceed 20% throughout the series. Therefore, the K/I ratio can be used as a reliable proxy of mineralogical changes. Based on the K/I ratio and the associated SiZer map, two major changes are observed during: 1) the Davoei Zone (Lower Pliensbachian; interval Ⓐ on Fig. 3), and; 2) the Spinatum Zone (Late Pliensbachian; interval Ⓑ on Fig. 3). Minor changes are visible: 1) around the Sinemurian-Pliensbachian boundary (interval ① on Fig. 3), and; 2) during the Margaritatus Zone, where three cycles are observed within the Stokesi (interval ② on Fig. 3) Subnodosus (interval ③ on Fig. 3) and Gibbosus (interval ④ on Fig. 3) Subzones. Both major and minor changes of the K/I ratio are observed with the SiZer analysis that statistically validate their occurrence.

4.2.2 Montcornet borehole (North Paris Basin)

Similar clay mineral assemblages are recognised at Montcornet, including kaolinite (2-54%), illite (9-58%), IS R1 (0-19 %), and chlorite (5-31%; Fig. 4). Two intervals showing smectite (up to 78%) are however identified during the Ibex Zone (interval ① on Figure 4) and before and during the "Grès Médioliasiques" Fm (interval ② on Fig. 4). The K/I ratio shows three major changes during the Pliensbachian: 1) around the Ibex-Davoei transition (interval Ⓐ on Fig. 4); 2) after the Margaritatus Zone (interval Ⓑ on Fig. 4), and; 3) during the "Grès Médioliasiques" Fm (interval Ⓒ on Fig. 4). The first two changes in the K/I ratio are validated by the SiZer analysis. The net and brief increase of the K/I ratio during the "Grès Médioliasiques" is associated to a marked lithological change expressed by the appearance of bioclastic limestones with reworked mud clasts (772.4-776.8 m), characteristic of more proximal and high-energy facies (Fig. 2). SEM observations have been performed on one bioclastic limestone bed (772.75 m) and reveal typical authigenic vermiform kaolinite in the

239 porosity (Fig. 5 A-C). Comparison has been made with one kaolinite-rich sample from
240 claystone at 812 m, considered as representative of detrital clayey sediments, where only typical
241 detrital shapes for clay particles have been observed, associated with rare calcitic bioclasts and
242 framboidal pyrite (Fig. 5 D).

243 *4.2.3 Additional sections (Corbigny, South Paris Basin; Charmouth, Wessex Basin)*

244 Computed K/I ratio from clay mineralogy data of the Corbigny section (see Dera, 2009)
245 shows low values during the Jamesoni and Ibex Zones and an increase during the Davoei Zone
246 (Fig. 6). In the Charmouth section, a low K/I ratio is also registered during the Jamesoni Zone,
247 while a slight increase starts in the Ibex Zone (Fig. 6). No data are currently available above
248 this level.

249

250 4.3 Carbon and oxygen isotope geochemistry (Montcornet borehole)

251 The bulk carbonate carbon isotope ($\delta^{13}C_{carb}$) signal recorded through the Pliensbachian
252 shows several significant changes (Fig. 3). A negative excursion of at least 1‰ (from 1.1‰ to
253 0‰) is observed between 929.4 m and 908 m from the Raricostatum Zone (Upper Sinemurian)
254 to an undefined zone between the Jamesoni and Ibex Zones (Lower Pliensbachian). A recovery
255 phase between 908 m and 892 m is marked by a positive trend with values which are going up
256 from 0‰ to 1.5‰, covering the possible upper Jamesoni Zone and of the lower Ibex Zone. The
257 Valdani Subzone (Ibex Zone) is characterised by a plateau from 892 m to 878 m with values
258 around 1.5‰. A second positive shift around 2‰ is observed between 878 m and 869.5 m from
259 the top of the Valdani Subzone and the top of the Ibex - lowermost part of the Davoei Zone,
260 before values decrease to 1.5‰ between 869.5 m and 866 m. Then a first negative shift with an
261 amplitude of 1.8‰ is observed between 866 m and 862.5 m (Maculatum Subzone, Davoei
262 Zone) followed by a low rebound from 862.5 m to 854m with values ranging from -0.25‰ to

263 0.25‰ (Capricornus and lower Figulinum Subzones, Davoei Zone). A second strong decrease
264 (at least -3‰) is observed between 854 m and 846 m in the Figulinum Subzone (Davoei Zone)
265 and keep fluctuating between -0.5‰ and -4‰ to 794 m. From 794 m, $\delta^{13}C$ values increase to
266 0.6‰ and fluctuate up to 1.2‰ to 782 m. Then, values slightly decrease down to 0.4‰ (773 m)
267 and increase to 1.6‰ upward. From 766m, a net decrease of values is marked by two steps with
268 the first one going down to 0‰ and the second one to -4‰.

269 The $\delta^{18}O_{carb}$ signal recorded from the bulk carbonate of Montcornet shows more
270 scattered values, yet some trends are observed and detailed in the supplementary material
271 (Suppl. Mat. Fig. 2). Values range from -6.8 to -1.7‰. No covariation is visible between carbon
272 and oxygen isotope data.

273

274 # 5. Discussion

275 ## 5.1. Influence of diagenesis

276 ### *5.1.1 Clay mineral diagenesis*

277 Lower Jurassic deposits from the Paris Basin are recognised to have sustained a low to
278 moderate burial diagenesis as shown by apatite fission tracks indicating a burial temperature
279 slightly greater than 60°C (Blaise et al., 2014).

280 At Montcornet, several lines of evidence including the occurrence of R0 type illite-
281 smectite mixed-layer (IS R0) in two intervals and mean T_{max} values below 430°C indicating
282 immature organic matter (Disnar et al., 1996), confirm a weak influence of thermal diagenesis
283 linked to burial. IS R0 are known to be particularly sensitive to burial diagenesis and transform
284 into IS R1 by illitisation processes with temperatures over 60-70°C (Merriman and Frey, 1999;
285 Lanson et al., 2009; Środoń et al., 2009; Dellisanti et al., 2010).

In the Sancerre borehole, the influence of burial diagenesis on clay assemblages is more questionable as IS R0 have not been identified. These minerals were either absent during sedimentation or have been transformed through incipient illitisation processes. However, mean Tmax values below 435°C indicate also an organic matter immaturity in the south of the Paris Basin (Hermoso et al., 2012). Consequently, as the occurrence of IS R0 is consistent with such T_{max} values (Dellisanti et al., 2010), these minerals were likely absent during sedimentation.

The kaolinite/illite ratio decreases with depth in all investigated sites (Figs. 3,4 and 6). This observation could raise the question of a potential illitisation of kaolinite associated to burial diagenesis (Ruffell et al., 2002; Worden and Morad, 2003). In such cases, illitisation of kaolinite with depth is generally progressive, while in the two studied boreholes the observed decrease of kaolinite is abrupt, rather indicating a palaeoenvironmental control. In addition, in the two boreholes, the main striking feature is the coeval decrease of the K/I ratio during the same ammonite biozone (i.e. Davoei Zone; Figs. 3 and 4). If the decrease of kaolinite with depth had been triggered by burial diagenesis, alteration at the same a stratigraphic horizon in different locations would have been an unlikely outcome. We suggest therefore that in both boreholes the influence of burial diagenesis on the clay mineral assemblages is negligible.

The occurrence of authigenic kaolinite is open to discussion as it is commonly associated with porous rocks such as limestone and sandstone. This mineral grows in pore spaces during eo- and meso-diagenesis by flushing of meteoric waters (Lanson et al., 2002; Worden and Morad, 2003). In both boreholes, there is no obvious relationship between lithology and clay mineralogy (Figs. 3 and 4). However, in a bioclastic limestone bed at 772.75 m in the Montcornet borehole, a high proportion of kaolinite (up to 55%) characterises the clay fraction (Figs. 2 and 4). Scanning Electronic Microscopy (SEM) observations revealed typical authigenic vermiform kaolinite in this sample (Fig. 5 A-C), suggesting that a large part of kaolinite content from this bed is related to fluid circulation. Other SEM observations from

311 clayey and limestone beds show common detrital shape morphologies, suggesting that kaolinite
312 formed by authigenesis is restricted to only one porous interval (Fig. 5C).

313 *5.1.2 Influence of diagenesis on the isotopic signal*

314 The carbonate fraction of the Pliensbachian marl and claystone of the Montcornet
315 borehole is a mixture of cemented micro-crystalline calcite (micrite) and thin bioclasts; these
316 were avoided in the process of microsampling. Measured isotopic composition of calcite in bulk
317 rocks ranges from -4.2 to 2.7 ‰ for the $\delta^{13}C$ and from -6.8to -1.7 ‰ for the $\delta^{18}O$, and are
318 consistent with values previously published from other Pliensbachian and Toarcian sections
319 (Jenkyns et al., 2002; Silva et al., 2011; Léonide et al., 2012; Hermoso et al., 2013; Duarte et
320 al., 2014). In Jurassic claystones, characterised by poor permeability and low burial
321 temperatures, the primary carbon isotope signal is frequently well-preserved during early and
322 late diagenetic processes (e.g. Hermoso et al., 2009; Lavastre et al., 2011; Pellenard et al.,
323 2014). Similar coeval $\delta^{13}C_{carb}$ fluctuations recognised in other Pliensbachian series well-dated
324 by ammonites (e.g. Silva et al., 2011; Duarte et al., 2014) highlight the negligible influence of
325 diagenesis. However, scattered and anomalous negative values of $\delta^{13}C_{carb}$ are observed
326 throughout a very argillaceous interval between 789 m and 862 m, corresponding to the Late
327 Pliensbachian (Davoei and Margaritatus Zones). This interval contains frequent red nodules of
328 siderite with occasional Zn-mineralisation (sphalerite), (Fig. 2) likely due to reducing
329 conditions occurring during early diagenesis, even if late fluid circulations cannot be ruled out.
330 The disturbed $\delta^{13}C_{carb}$ signal obtained here which prevents the use of bulk carbonate carbon
331 isotope values for palaeoenvironmental reconstructions is mainly explained by low carbonate
332 contents.

333 The $\delta^{18}O_{carb}$ values in the Montcornet borehole are scattered, particularly in the 789 m
334 to 862 m siderite-nodule-bearing interval indicating thorough fluid circulation.. Trends are yet

observed at the base and the top of the borehole with higher values between 905 m and 890 m (base Ibex Zone) and 790 m and 775 m (Spinatum Zone?), which may suggest cooler temperatures during these two intervals. Nevertheless, bulk oxygen isotope data have to be used with caution here as they are much more sensitive to diagenetic effects than carbon isotope data (Marshall, 1992; Jenkyns et al., 2002).

5.2. Significance of the clay mineral record

Clay mineral assemblages are composed of a mixture of illite, IS R1, occasional IS R0, kaolinite and chlorite, and this composition is a very common feature of Early Jurassic sediments from European basins (Delavenna et al., 1989; Deconinck and Bernoulli, 1991; Debrabant et al., 1992; Duarte, 1998; Deconinck et al., 2003; Jeans, 2006; Raucsik and Varga, 2008; Dera et al., 2009a; Brański, 2012; Lézin et al., 2013; Hermoso and Pellenard, 2014). These clay minerals are considered to be chiefly inherited from detrital sources, because burial diagenesis is low and authigenesis only observed in one porous interval. No evidence of major tectonic rejuvenation of landmasses is reported for the Pliensbachian in the Paris Basin, which is thought to have been broadly a quiescent period in an extensional subsidence context (Brunet and Le Pichon, 1982; Guillocheau et al., 2000; Beccaletto et al., 2011). Consequently, clay mineral supplies were likely controlled by variations in eustasy, climate, and sediment source area.

Clay mineralogy is partly dependent on the nature of weathered rocks outcropping on emerged landmasses, where it may originate from either contemporaneous soils or old sediments. Although proximal continental areas were the main sources, more distal sources could also be expected, because clay minerals are transportable over long distances by marine or aeolian currents. The main landmasses surrounding the Paris and the Wessex basins were the

London-Brabant Massif to the north prolonged by the Rhenish Massif eastward, the Bohemian Massif to the east, the Massif Central to the south prolonged by the Armorican Massif westward, the Cornubian-Welsh High and Irish Massif to the west and the Scottish Massif to the northwest (Figs. 1 and 7). Erosion of these emerged lands, mainly composed of Palaeozoic igneous, metamorphic and sedimentary rocks, would have favoured inputs of primary clay minerals such as illite or chlorite. Weathering of the crystalline basement, may have also provided IS R1, smectite (IS R0) and kaolinite. This latter mineral may be reworked from the basement sedimentary rocks together with illite and chlorite (Deconinck et al., 2003; Dera et al., 2009a).

5.2.1 Origin of smectite

Interestingly, smectite is only reported in the Montcornet borehole for the Ibex Zone and around the Pliensbachian-Toarcian transition. Differential sedimentation of clay minerals is responsible for the increase of kaolinite, commonly observed during regression phases in association with proximal facies, whereas smectite and mixed-layer minerals are more frequently recorded during associated with maximum flooding surfaces (Chamley, 1989; Ruffell et al., 2002; Pellenard and Deconinck, 2006; Godet et al., 2008). Inferred large-scale transgressive-regressive (T/R) facies cycles from European domains (Hardenbol et al., 1998; Jacquin et al., 1998) are reproduced on Figures 3 and 4. These so-called 'second-order' order T/R cycles (T4/R4, T5/R5) match well with the sedimentological pattern and depositional environments observed through the two boreholes, in particular for cycles defined in the Tethyan domains. A maximum flooding surface is reported within the lower Margaritatus Zone (Stokesi Subzone). Regressive maxima are at the top of the Ibex Zone for the Tethyan domains (or at the top of the Davoei Zone for the Boreal domains) and the top of the Spinatum Zone (Pliensbachian/Toarcian boundary). The Spinatum Zone was not recognised in the Montcornet borehole, but the bioclastic limestone beds between 772 and 777 m are attributed to an

384 equivalent of the "Grès Médioliasiques Fm" well known throughout the Paris Basin, dated to
385 the Spinatum Zone and corresponding to a regressive maxima (Hermoso et al., 2013; Brigaud
386 et al., 2014). Surprisingly, these regressive maxima correspond to the two smectite-rich
387 intervals with proportions reaching more than 50% (Fig. 4). Smectite was exclusively restricted
388 to the northern part of the Paris Basin until the Late Jurassic (Debrabant et al., 1992; Pellenard
389 and Deconinck, 2006), which suggests it likely originated from the London-Brabant and
390 Rhenish massifs. Compared to other massifs inherited from the Variscan orogeny, the London-
391 Brabant and Rhenish-Eiffel massifs including the Ardennaise platform should constitute
392 moderate and flat relief during the Jurassic. This morphology was favourable to the formation
393 of smectite-rich soils under semi-arid to temperate climates with strong seasonality (Chamley,
394 1989; Paquet and Clauer, 1997), whereas illite, chlorite and IS R1 could be formed on higher
395 relief with steeper slopes and less pronounced weathering. A reported regional uplift with
396 moderate average speed of unroofing of the London-Brabant and Rhenish-Eiffel massifs
397 throughout the Jurassic (Vercoutere and Van den Haute, 1993) may also have played a role for
398 denudation of relief and the peneplanation favourable for the storage of smectites. During
399 regressive phases, the smectite-rich soils from low relief landmass and previously smectite-rich
400 sediments stored on platforms were preferentially eroded, and are hypothesized to have
401 supplied adjacent areas of the basin (Fig. 7A). By contrast, during sea-level highstand, flooding
402 of the flat London-Brabant Massif prevented smectite-rich sedimentation in the Paris Basin
403 (Fig. 7B). This uncommon relationship between smectite sedimentation and low sea-level is
404 only observed in the north of the Paris Basin and the Boulonnais area from the Callovian to the
405 Tithonian (Schnyder et al., 2000; Pellenard and Deconinck, 2006; Deconinck and Baudin, 2008;
406 Hesselbo et al., 2009). The present study shows that as early as the Pliensbachian, the London-
407 Brabant Massif exhibited a flat morphology by comparison with other emerged landmasses.
408 Eustatic sea-level variations can thus explain here some regional clay mineralogical features,

409 but is insufficient to explain the several kaolinite changes, correlated between the four studied
410 sites.

411 *5.2.2 Significance of the K/I ratio*

412 The K/I ratio shows two main significant changes at the investigated localities: 1) a
413 sharp increase at the transition between the Ibex and Davoei Zones, and; 2) a decrease in the
414 Spinatum Zone (Fig. 6). The abrupt increase of the K/I ratio at the base of the Davoei Zone
415 coincides with the onset of the T5 2nd order transgressive cycle (Tethyan domains) and remains
416 high up to the top of the R5 regressive cycle (Figs. 3 and 4). Looking at large scale trends of
417 K/I ratio in the Sancerre and Montcornet boreholes, regressive facies trends are not
418 characterised by an increase of kaolinite but rather by a decrease (Ibex and Spinatum Zones),
419 and no evidence linking kaolinite maxima and regressive maxima can be identified. Kaolinite
420 variations and inferred K/I ratio are unlikely to be forced by a unique eustatic control.

421 Clay minerals are known to reflect climate through continental weathering and runoff
422 in modern environments and in deep time (Chamley, 1989; Hallam et al., 1991; Paquet and
423 Clauer, 1997; Thiry, 2000; Dera et al., 2009a). Kaolinite is preferentially formed at low latitudes
424 under hot and wet tropical climate, allowing strong hydrolysing processes to take effect (Paquet
425 and Clauer, 1997; Thiry, 2000). By contrast, chlorite and illite are formed in drier climates
426 where physical erosion prevails (Chamley, 1989). Therefore, many authors classically use
427 kaolinite as a reliable indicator of humid tropical climatic belt, whereas chlorite and illite are
428 used as proxies of cold and dry conditions or associated to arid environments. Evolution of clay
429 mineral assemblages from the Pliensbachian highlight covariation of kaolinite and chlorite
430 (Figs. 3 and 4), which is a very unusual feature and difficult to reconcile in terms of coeval
431 formation in a soil governed by a unique climate. Moreover, as discussed by Thiry (2000),
432 formation of kaolinite-rich laterite and erosion of clay into the oceanic domain require long
433 durations, estimated to more than 1 Myr. The studied area was located between 30° and 40° of

palaeolatitude (Thierry et al., 2000). On the basis of GCM models and lithological and palaeontological data, the region was subjected to humid to semi-arid climates and megamonsoonal conditions (Rees et al., 2000; Dera et al., 2009a). Evidence of contemporaneous kaolinite-rich soils surrounding basins in the north Tethyan basins has not been demonstrated, and some authors point to the reworking of kaolinite from Palaeozoic rocks instead as the main source (Hurst, 1985; Jeans, 2006). Kaolinite is, for example, reported in Devonian and Carboniferous rocks as detrital and/or authigenic mineral derived from closely emerged landmasses (Crasquin, 1983; Hillier et al., 2006; Shaw, 2006). The palaeogeography of the north Tethyan domains, as an archipelago with landmasses partly or completely drowned by an epicontinental sea, has also probably reinforced the high proportions of kaolinite in the studied basins by comparison with other basins. Periods of strong chemical and physical erosion by intensive runoff on these continents have therefore likely contributed to increase inherited kaolinite content of contemporaneous marine sediments, while illite and IS R1 corresponded to the background of the clay sedimentation. Therefore, we suggest that the K/I ratio is a reliable proxy to estimate the runoff on continents and inferred humidity/aridity changes that strongly influenced continental weathering during the Pliensbachian (cf. Ruffell et al., 2002).

5.2.3 Illite, chlorite and kaolinite sources

In the Montcornet and Sancerre boreholes, the clay fraction of the Pliensbachian sediments display unusual features: 1) chlorite is abundant reaching 20% on average, while Jurassic rocks from European sedimentary basins show generally at most 10% of chlorite in their clay fraction (e.g. Ruffell et al., 2002; Deconinck et al., 2003; Jeans, 2006; Pellenard and Deconinck, 2006; Schnyder et al., 2006); 2) parallel changes in illite and chlorite proportions are not observed, whereas these primary minerals usually show coeval changes in most sedimentary series, and: 3) instead a co-variation of kaolinite and chlorite is surprisingly highlighted here, even though these two minerals cannot be formed under the same climatic

conditions. This coeval kaolinite- and chlorite-rich composition suggests either two distinct sources or a common detrital source with both kaolinite and chlorite inherited from ancient rocks.

The similar temporal evolution of kaolinite and chlorite suggest a common source. The absence of co-variations of chlorite and illite and the co-variation of kaolinite and chlorite could thus be explained by the reworking of authigenic chlorite and kaolinite formed in pore-spaces of old sandstones notably described in the boreal domain along the Fennoscandian Shield (Mørk et al., 2003; Dera et al., 2009a). We suggest therefore that at least a part of kaolinite and chlorite can be considered as tracers of boreal sources, specifically during periods of high sea-level, when the London-Brabant Massif was flooded (Fig. 7B). By contrast, during periods of sea-level fall, kaolinite and chlorite from boreal domains were likely trapped between the Fennoscandian Shield and the London-Brabant Massif, this latter feeding the northern part of the Paris Basin with smectite (Montcornet, Fig. 7A). High proportions of kaolinite and chlorite occur throughout the Pliensbachian succession of the Cleveland Basin (Jeans, 2006), suggesting continuous input of reworked kaolinite and chlorite from boreal domains, an observation that strengthens this interpretation (Fig. 7).

5.3. Climatic events and runoff during the Pliensbachian

5.3.1 Relationships between clay mineralogy and C-O-isotopes

In order to test relationships between clay mineral changes and carbon cycle events in the Tethyan domain, correlations have been attempted between the four studied sections using ammonite biostratigraphy and carbon-isotope chemostratigraphy and by comparing the K/I ratio, considered here as a proxy for runoff on land, to significant negative and positive excursions in carbon isotopes (Fig. 6). Sancerre and Montcornet boreholes cover the top

483 Sinemurian to lowermost Toarcian in the Paris Basin, while Charmouth (Wessex Basin) and
484 Corbigny (Paris Basin) sections provide additional data for the lower Pliensbachian.

485 During the Late Sinemurian and most of the Early Pliensbachian (up to the Ibex Zone),
486 a low K/I ratio is observed. At the Sinemurian-Pliensbachian boundary, a weak increase in the
487 K/I ratio is recorded at Sancerre (Fig. 6). A coeval increase of kaolinite content is consistently
488 reported in the Lusitanian Basin (Caniço et al., 2015). This trend is not observed at Montcornet
489 and Charmouth (Fig. 6). It could be explained by either a condensation or hiatus in the
490 Sinemurian-Pliensbachian boundary interval of the two latter sections. Indeed, the Taylori
491 Subzone (first Subzone of the Jamesoni Zone) is not recognised at Montcornet and a hiatus is
492 highlighted at Charmouth (Hesselbo and Jenkyns, 1995). This mineralogical change occurred
493 within a negative carbon isotope excursion measured on organic matter in the Sancerre borehole
494 (Peti et al., submitted) and on bulk carbonate at Montcornet (Fig. 6). This negative excursion,
495 at the so-called Sinemurian-Pliensbachian Boundary Event (SPBE), was identified from
496 belemnite carbon-isotope data and organic matter/wood $\delta^{13}C$ in U.K. basins (Korte and
497 Hesselbo, 2011; Price et al., 2016; Ruhl et al., 2016) and can also be seen in earlier compilations
498 (Jenkyns et al., 2002). The same event has been described in the Lusitanian Basin (Duarte et
499 al., 2014), the Asturian Basin (Armendáriz et al., 2012; Gómez et al., 2016) and the Trento
500 platform (Franceschi et al., 2014). This negative shift is reported Fig. 8 from the belemnite
501 carbon isotope compilation of Martinez and Dera (2015).

502 From the top of the Ibex Zone to the lower Davoei Zone, the K/I ratio dramatically
503 increase in Montcornet and Sancerre (Fig. 6). This major mineralogical change coincides with
504 a decrease in $\delta^{13}C_{org}$ and $\delta^{13}C_{carb}$ values (Fig. 6) and follows a sea-level lowstand expressed by
505 the occurrence of smectites on the southern borders of the London-Brabant Massif (LBM). This
506 major mineralogical change is consistent with the general increase of the kaolinite input into
507 the NW European domain within the Davoei Zone (Dera et al., 2009a). The K/I increase is also

concomitant with more negative $\delta^{18}O$ values measured from belemnite rostra, suggesting warming of sea water (Rosales et al., 2004; Dera et al., 2011a; Armendáriz et al., 2012; Martinez and Dera, 2015; Gómez et al., 2016, Fig. 8).

From the top of the Davoei Zone to the top of the Margaritatus Zone, the K/I ratio remains high at Sancerre and Montcornet with slight variations following three cycles in both boreholes (Fig. 6). These clay mineral cycles likely reflect variations of the runoff triggered by climate in the Milankovitch frequency-band as observed in some Cretaceous sedimentary series (Moiroud et al., 2012; Ghirardi et al., 2014). These runoff cycles are roughly correlated with carbon isotope cycles from organic matter in the Sancerre borehole.

The upper Pliensbachian (Spinatum Zone) is characterised by a sharp decrease of the K/I ratio (Fig. 6), also reported by Dera et al. (2009a). This change precedes an increase in $\delta^{13}C_{carb}$ values and is coeval with maximal $\delta^{18}O$ values. Similar high $\delta^{18}O$ values, recorded in the Lusitanian Basin (Oliveira et al., 2006; Suan et al., 2010), in Spain (Rosales et al., 2004; Gómez et al., 2016), in the Cleveland Basin (Korte and Hesselbo, 2011), and in the Western Carpathians (Arabas and Schlögl, 2015), suggest that low runoff occurred during a cooler period (Fig. 8).

5.3.2 Periods of enhanced runoff

Using the K/I ratio as a tracer of humid conditions, at least three periods of enhanced runoff are recognised throughout the Pliensbachian (Fig. 8): 1) the Sinemurian-Pliensbachian boundary, 2) the Lower/Upper Pliensbachian transition (Davoei/Margaritatus Zones), 3) the Subnodosus Subzone (Margaritatus Zone, Upper Pliensbachian).

A long-lasting $\delta^{13}C$ negative excursion of ~2‰, corresponding to the SPBE, encompasses the Sinemurian-Pliensbachian boundary. This carbon excursion recorded in marine carbonates and organic matter has been reported in many localities from the Tethyan

532 domain suggesting a supra-regional or global event (Korte and Hesselbo, 2011). A source of
533 isotopically light CO_2 injected into the ocean-atmosphere system is required to explain this 2‰
534 amplitude negative carbon-isotope excursion, likely suggesting either a volcanic contribution,
535 as proposed by Ruhl et al. (2016), or methane release, as discussed for the CIE (Carbon Isotope
536 Excursion) of the T-OAE (Hesselbo et al., 2000a; Hesselbo et al., 2007; Hesselbo and
537 Pieńkowski, 2011; Suan et al., 2011). A hyperthermal event was highlighted during the T-OAE
538 associated to CO_2 release triggered by Karoo-Ferrar volcanic activity (Pàlfy and Smith, 2000;
539 Jourdan et al., 2008) and/or methane hydrate reservoir disruption (Hesselbo et al., 2000a;
540 Jenkyns, 2010). The subsequent high pCO_2 favoured: 1) concomitant large organic matter
541 accumulations (black-shale deposits) (e.g. Jenkyns, 1988, 2010; Baudin et al., 1990), and; 2)
542 runoff and continental weathering increases, expressed by a set of isotope data (Sr, Os, Ca ...)
543 (Jones and Jenkyns, 2001, Bailey et al., 2003; Cohen et al., 2004; Brazier et al., 2015; Ruhl et
544 al., 2016) and sedimentological evidence, including change in clay mineral proportions
545 (Hermoso and Pellenard, 2014). A similar increase in pCO_2 is interpreted by the $\Delta^{13}C$ ($\delta^{13}C_{carb}$-
546 $\delta^{13}C_{org}$) during the SPBE (van de Schootbrugge et al., 2005). Organic matter-rich sediment
547 including black shale was also deposited in dysoxic to anoxic environments during the latest
548 Sinemurian (Rosales et al., 2004; Boussaha et al., 2014, Duarte et al., 2014). Besides the
549 kaolinite enrichment observed in this study, proxies of continental weathering and runoff are
550 also reported, including, for example, eutrophic conditions linked to higher nutrient input from
551 continents preventing the widespread occurrence of the *Lithiotis* fauna (Franceschi et al., 2014).
552 Temperature reconstructions for the SPBE are still debated but no evidence of hyperthermal
553 temperatures has been described, in contrast to the T-OAE. A warm period is suggested during
554 the latest Sinemurian based on belemnites from the Asturian Basin (Gómez et al., 2016),
555 whereas a slight cooling trend is recorded by belemnites and bivalves in the Cleveland Basin
556 (Korte and Hesselbo, 2011). However, cool bottom water temperatures described in the

557 Cleveland Basin may reflect local deep water conditions and bias temperature reconstruction
558 of this period (Korte and Hesselbo, 2011). This event was rather interpreted as a greenhouse
559 interval (Korte and Hesselbo, 2011), consistent with a humid climate and consequently
560 enhanced runoff on landmasses, as supported by our data.

561 The Lower/Upper Pliensbachian transition (e.g. Davoei Zone-Stokesi Subzone) may
562 display the most obvious change in runoff conditions during the Pliensbachian with a
563 generalised and dramatic increase in the kaolinite input to the NW European Basins (Fig. 8).
564 Interestingly, this period coincides with: 1) a slight change in the $^{87}Sr/^{86}Sr$ curve characterised
565 by a plateau, suggesting enhanced continental weathering, while a broad decrease of $^{87}Sr/^{86}Sr$
566 values is recognised throughout the Pliensbachian, hypothetically linked to sea-floor spreading
567 (Jones et al., 1994; Jones and Jenkyns, 2001); 2) rising sea temperatures inferred from oxygen
568 isotope belemnite data (Dera et al., 2009b; 2011a; Martinez and Dera, 2015; Gómez et al.,
569 2016); 3) occasional black shale deposits in the Lusitanian Basin (Silva and Duarte, 2015); 4)
570 a decrease in ammonite species richness observed in the NW European and Mediterranean
571 domains likely triggered by warming (Dommergues et al., 2009).

572 These lines of evidence highlight warmer and more humid conditions at the base of the
573 Davoei Zone. However, this interval is also characterised by a change in the detrital supply
574 shifting to boreal sources (see section 5.2.3), and a suggested change in water mass circulation
575 in the NW European domain. In the Davoei Zone, more radiogenic εNd values recorded in fish
576 teeth imply an input of water mass affected by young and more radiogenic rocks what may
577 correspond to sources from the Panthalassa ocean or more likely from low latitudes of the
578 Tethys Ocean (Dera et al., 2009b; Dera et al., 2015). This apparent paradox between detrital
579 flux from the Fennoscandian Shield and radiogenic water input originating from the south may
580 be explained by a rising sea-level favouring connections between sedimentary basins and a new
581 current pattern (Fig. 7). The subsequent flooding of the London-Brabant Massif would allow

582 kaolinite and chlorite inputs into the Paris and Wessex basins from the north. These
583 palaeoceanographic and palaeogeographic changes are consistent with mixing of ammonite
584 faunas from euro-boreal domains recognised during the Davoei Zone (Dera et al., 2011b).
585 Finally, the Lower/Upper Pliensbachian transition is characterised by two major environmental
586 disruptions: 1) a warming episode associated to enhanced runoff, and; 2) rising sea-level and
587 palaeoceanographic changes. These conditions contributed to explain the dramatic clay
588 mineralogical change observed in NW European domains.

589 In the Margaritatus Zone, the K/I ratio displays weak fluctuations likely triggered by
590 variability in runoff intensity. The maximum values (i.e. Subnodosus Subzone), coincide with
591 the occurrence of organic matter-rich sediment and black shale deposits reported as the Late
592 Pliensbachian Organic-Rich Preservation Interval (OMPI; Rosales et al., 2004; Silva et al.,
593 2011; Armendáriz et al., 2012; Caruthers et al., 2014; Silva and Duarte, 2015; Neumeister et
594 al., 2015). Maximal runoff within Subnodosus Subzone likely triggered an increase in organic
595 productivity through the associated increase in the nutrient supply.

596

597 *5.3.3 Glacio-eustasy during the Pliensbachian?*

598 The possibility for glacio-eustasy should be addressed because smectite events in the
599 north Paris Basin clearly indicate emersion of the London Brabant Massif (LBM) during sea-
600 level fall, while the absence of this mineral highlights its flooding during sea-level rise (Figs. 7
601 and 8). Such a great palaeogeographic change likely resulted from the flatter and lower
602 topography of the LBM compared to other Palaeozoic massifs because of its external position
603 in the Variscan belt. Alternating emersion and flooding of the LBM with relatively short
604 durations (i.e. <1 Myr) and high amplitude variations of the sea-level, at least several tens of
605 metres, appears more consistent with a glacio-eustasy model than a regional uplift. Indeed

606 regional uplift associated to the Cimmerian tectonic phases, described for the LBM, seems have
607 been progressive with moderate speed of unroofing throughout the Jurassic from apatite fission
608 track data (Vercoutere and Van den Haute 1993). The smectite events are recorded within the
609 Ibex and Spinatum Zones, which correspond to cooler intervals as expressed in oxygen isotope
610 data (Fig. 8 and Suppl. Mat. Fig. 1). This is particularly clear in the Spinatum Zone, for which
611 time ice-cap growth has been previously suggested from sedimentological and isotope data
612 (Price, 1999; Suan et al., 2011, Dera et al., 2011a, 2011b; Korte and Hesselbo, 2011; Arabas
613 and Schlögl, 2015). This inference is also consistent with a relatively low pCO_2 (around 900
614 ppm) inferred from stomatal density from Araucariacea leaves (Steinthorsdottir and Vajda,
615 2015). In this cooler interval, the K/I ratio dramatically drops suggesting reduced humidity,
616 slowing down of the water cycle, and subsequent low runoff (Fig. 8). Combined with the sea-
617 level fall inferred from the uppermost part of the Pliensbachian, this situation strengthens a
618 glacio-eustatic control. A similar situation occurred from the probably topmost part of the
619 Jamesoni Zone to the lower part of the Ibex Zone, where low K/I ratio and smectite occurrence
620 are observed together with higher values in bulk $\delta^{18}O_{carb}$ within a regressive trend and a low
621 stand of sea-level (Fig. 8 and Suppl. Mat. Fig. 2). These coincident changes are consistent with
622 the formation of ice at high latitudes during the interval that spans the Ibex Zone, although
623 belemnite oxygen isotope data are more scattered and do not show any clear cooling (Fig. 8).
624 Changes in the SMOW values during the cold snap and the subsequent deglaciation, providing
625 fresh water input and salinity variations, could also be responsible for the scattered oxygen
626 isotope data. Recent isotope data from belemnite in the Dorset (U.K.) are consistent with a
627 relatively cold Jamesoni-Ibex interval compared to the warmer Davoei interval (Price et al.,
628 2016). The following warming and deglaciation, combined with the sea level rise, likely
629 enhanced runoff and reworking of ancient kaolinite and chlorite-bearing sediments and rocks
630 from the Fennoscandian Shield. This climatic story is consistent with oxygen isotope data

631 published in the Basque-Cantabrian and Asturian Basins (Rosales et al., 2006; Armendáriz et
632 al., 2012).

633

634 6. Conclusions

635 Clay mineral and paired carbon-oxygen-isotope data have been generated from two boreholes
636 in the Paris Basin representing an interval from the latest Sinemurian to the earliest Toarcian,
637 with additional mineralogical data from sections in the Paris and Wessex Basins. The diversity
638 of clay assemblages results from the complex interplay of several detrital sources, sea-level
639 change, seaway circulation, and runoff. The following features interpreted in terms of climate
640 and palaeoceanographic changes are highlighted:

641 - Increasing kaolinite/illite ratio characterises periods of enhanced runoff, during: i) the
642 Sinemurian-Pliensbachian transition associated with a negative carbon excursion (SPBE); ii)
643 the Early/Late Pliensbachian transition (Davoei Zone-Stokesi Subzone), and; iii) the
644 Subnodosus Subzone (Late Pliensbachian, Margaritatus Zone). These periods correspond to
645 warm and humid climates, favouring continental weathering and subsequent black shale
646 deposition. By contrast, cooler periods with low runoff occurred during the Jamesoni - Ibex and
647 the Spinatum Zones.

648 - The influence of climate forcing on clay assemblages is magnified by palaeoceanographic
649 changes and sea level fluctuations. A dramatic change in clay mineralogy is notably observed
650 for the Davoei Zone, characterised by kaolinite and chlorite-rich sedimentation. We suggest
651 that these minerals were likely reworked from ancient sediments and rocks from the
652 Fennoscandian Shield during a high sea-level period favouring connections between
653 sedimentary basins and flooding of the London Brabant Massif. By contrast, this massif was
654 emerged during periods of sea-level lowstand and acted as a topographic barrier.

- Two smectite-rich intervals occurred in the north Paris Basin during the two periods of sea-level lowstand (Ibex and Spinatum Zones). These features are limited to the margin of the London Brabant Massif, which was a unique source of smectite. These smectite events highlight recurrent emersions of the London Brabant Massif, characterised by a flat and low topography, and suggest significant amplitude of the sea-level fluctuation that could be explained by glacioeustasy. Smectite-rich intervals in the north Paris Basin may thus emphasize continental ice growth at times during the Early Jurassic (i.e. late Jamesoni/early Ibex Zones and Spinatum Zone).

Acknowledgements

The study was supported by the "Agence Nationale pour la Gestion des Déchets Radioactifs" (Andra—French National Radioactive Waste Management Agency). We are grateful to P. Landrein and C. Aurière for access to the Andra core store and P. Neige for Toarcian ammonite determination. The authors thank S. Bodin and an anonymous reviewer for their helpful comments.

References

Al-Suwaidi, A.H., Angelozzi, G.N., Baudin, F., Damborenea, S.E., Hesselbo, S.P., Jenkyns, H.C., Manceñido, M.O., Riccardi, A.C., 2010. First record of the Early Toarcian Oceanic Anoxic Event from the Southern Hemisphere, Neuquén Basin, Argentina. Journal of the Geological Society 167, 633-636.

676 Arabas, A., Schlögl, J., 2015. Oxygen and carbon isotope records of Lower-Middle Jurassic
677 belemnite rostra and marine carbonates from the Pieniny Klippen Belt (Carpathians).
678 Abstract Book of 31st IAS Meeting of Sedimentology, Kraków, p.38.

679 Armendáriz, M., Rosales, I., Bádenas, B., Aurell, M., García-Ramos, J.C., Piñuela, L., 2012.
680 High-resolution chemostratigraphic records from Lower Pliensbachian belemnites:
681 Palaeoclimatic perturbations, organic facies and water mass exchange (Asturian basin,
682 northern Spain). Palaeogeography, Palaeoclimatology, Palaeoecology 333-334, 178-191.

683 Bailey, T.R., Rosenthal, Y., McArthur, J.M., van de Schootbrugge, B., 2003.
684 Paleoceanographic changes of the Late Pliensbachian - Early Toarcian interval: a possible
685 link to the genesis of an Oceanic Anoxic Event. Earth Planetary Science Letters 212, 307-
686 320.

687 Baudin, F., Herbin, J.P., Bassoullet, J.P., Dercourt, J., Lachkar, G., Manivit, H., Renard, M.,
688 1990. Distribution of organic matter during the Toarcian in the Mediterranean Tethys and
689 Middle East. AAPG Special Vol. 6, 73-91.

690 Beccaletto, L., Hanot, F., Serrano, O., Marc, S., 2011. Overview of the subsurface structural
691 pattern of the Paris Basin (France): Insights from the reprocessing and interpretation of
692 regional seismic lines. Marine and Petroleum Geology 28, 861-879.

693 Bjerrum, C.J., Surlyk, F., Callomon, J.H., Slingerland, R.L., 2001. Numerical
694 paleoceanographic study of the early Jurassic transcontinental Laurasian Seaway.
695 Paleoceanography 16, 390-404.

696 Blaise, T., Barbarand, J., Kars, M., Ploquin, F., Aubourg, C., Brigaud, B., Cathelineau, M., El
697 Albani, A., Gautheron, C., Izart, A., Janots, D., Michels, R., Pagel, M., Pozzi, J.-P.,
698 Boiron, M.-C., Landrein, P., 2014. Reconstruction of low burial (<100 °C) in sedimentary

basins: a comparison of geothermometer in the intracontinental Paris Basin. Marine and Petroleum Geology 53, 71-87.

Boussaha, M., Pittet, B., Mattioli, E., Duarte, L.V., 2014. Spatial characterization of the late Sinemurian (Early Jurassic) palaeoenvironments in the Lusitanian Basin. Palaeogeography, Palaeoclimatology, Palaeoecology 409, 320-339.

Brański, P., 2012. The mineralogical record of the Early Toarcian stepwise climate changes and other environmental variations (Ciechocinek Formation, Polish Basin). Volumina Jurassica 10, 1-24.

Brazier, J.-M., Suan, G., Tacail, T., Simon, L., Martin, J.E., Mattioli, E., Balter, V., 2015. Calcium isotope evidence for dramatic increase of continental weathering during the Toarcian oceanic anoxic event (Early Jurassic). Earth and Planetary Science Letters 411, 164-176.

Brigaud, B., Vincent, B., Carpentier, C., Robin, C., Guillocheau, F., Yven, B., Huret, E., 2014. Growth and demise of the Jurassic carbonate platform in the intracratonic Paris Basin (France): Interplay of climate change, eustasy and tectonics. Marine and Petroleum Geology 53, 3-29.

Brunet, M.-F., Le Pichon, X., 1982. Subsidence of the Paris Basin. Journal of the Geophysical Society 87, 8547-8560.

Caniço, A., Duarte, L.V., Silva, R.L., Rocha, F., Mendonça Filho, J.G., 2015. Minerals and clay minerals assemblages in organic-rich facies: the case study of the Sinemurian-Pliensbachian carbonate deposits of the western Lusitanian Basin (Portugal). Geophysical Research Abstracts 17, EGU 2015-4807.

721 Caruthers, A.H., Smith, P.L., Gröcke, D.R., 2014. The Pliensbachian–Toarcian (Early Jurassic)
722 extinction: A North American perspective. Geological Society of America Special Papers
723 505, 225-243.

724 Chamley, H., 1989. Clay Sedimentology. Springer Verlag, Berlin, 623 p.

725 Cohen, A.S., Coe, A.L., Harding, S.M., Schwark, L., 2004. Osmium isotope evidence for the
726 regulation of atmospheric CO2 by continental weathering. Geology 32, 157-160.

727 Crasquin, S., 1983. Ostracodes viséens du Nord de la France (Etude paléontologique et analyse
728 de la fraction argileuse). Annales de la Société Géologique du Nord 102, 191-204.

729 Debrabant, P., Chamley, H., Deconinck, J.-F., Récourt, P., Trouiller, A., 1992. Clay
730 sedimentology, mineralogy and chemistry of Mesozoic sediments drilled in the northern
731 Paris Basin. Scientific Drilling 3, 138-152.

732 Deconinck, J.-F., Baudin, F., 2008. Les dépôts du Kimméridgien et du Tithonien du nord-ouest
733 du Bassin de Paris (Haute-Normandie, Boulonnais). Annales de la Société Géologique du
734 Nord 15, 77-90.

735 Deconinck, J.-F., Bernoulli, D., 1991. Clay mineral assemblages of Mesozoic pelagic and flysch
736 sediments of the Lombardian Basin (Southern Alps): implications for palaeotectonics,
737 palaeoclimate and diagenesis. Geologische Rundschau 80, 1-17.

738 Deconinck, J.-F., Hesselbo, S.P., Debuisser, N., Averbuch, O., Baudin, F., Bessa, J., 2003.
739 Environmental controls on clay mineralogy of an Early Jurassic mudrock (Blue Lias
740 Formation, southern England). International Journal of Earth Sciences 92, 255-266.

741 Delavenna, M.-F., Steinberg, M., Trauth, N., Holtzapffel, T., 1989. Influence des cycles
742 eustatiques et de la tectonique synsédimentaire sur la minéralogie du Lias et du Dogger

743 du forage de Sancerre-Couy (Cher). Programme Géologie profonde de la France.
744 Comptes Rendus de l'Académie des Sciences 308, 111-116.

745 Dellisanti, F., Pini, G.A., Baudin, F., 2010. Use of T_{max} as a thermal maturity indicator in
746 orogenic successions and comparison with clay mineral evolution. Clay minerals 45, 115-
747 130.

748 Dera, G., 2009. Le rôle des changements paléoclimatiques sur l'évolution de la biodiversité au
749 Pliensbachien et au Toarcien. Ph.D. Unpubl. Thesis, University of Burgundy, Dijon,
750 France.

751 Dera, G., Pellenard, P., Neige, P., Deconinck, J.-F., Pucéat, E., Dommergues, J.-L., 2009a.
752 Distribution of clay minerals in Early Jurassic Peritethyan seas: Palaeoclimatic
753 significance inferred from multiproxy comparisons. Palaeogeography,
754 Palaeoclimatology, Palaeoecology 271, 39-51.

755 Dera, G., Pucéat, E., Pellenard, P., Neige, P., Delsate, D., Joachimski, M.M., Reisberg, L.,
756 Martinez, M., 2009b. Water mass exchange and variations in seawater temperature in the
757 NW Tethys during the Early Jurassic: Evidence from neodymium and oxygen isotopes of
758 fish teeth and belemnites. Earth and Planetary Science Letters 286, 198-207.

759 Dera, G., Brigaud, B., Monna, F., Laffont, R., Pucéat, E., Deconinck, J.-F., Pellenard, P.,
760 Joachimski, M.M., Durlet, C., 2011a. Climatic ups and downs in a disturbed Jurassic
761 world. Geology 39, 215-218.

762 Dera, G., Neige, P., Dommergues, J.-L., Brayard, A., 2011b. Ammonite paleobiogeography
763 during the Pliensbachian–Toarcian crisis (Early Jurassic) reflecting paleoclimate, eustasy,
764 and extinctions. Global and Planetary Change 78, 92-105.

765 Dera, G., Prunier, J., Smith, P.L., Haggart, J.W., Popov, E., Guzhov, A., Rogov, M., Delsate,
766 D., Thies, D., Cuny, G., Pucéat, E., Charbonnier, G., Bayon, G., 2015. Nd isotope
767 constraints on ocean circulation, paleoclimate, and continental drainage during the
768 Jurassic breakup of Pangea. Gondwana Research 27, 1599-1615.

769 Disnar, J.R., Le Strat, P., Farjanel, G., Fikri, A., 1996. Sédimentation de la matière organique
770 dans le nord-est du Bassin de Paris: conséquences sur le dépôt des argilites carbonées du
771 Toarcien inférieur. Chemical Geology 131, 15-35.

772 Dommergues, J.-L., Fara, E., Meister, C., 2009. Ammonite diversity and its
773 palaeobiogeographical structure during the early Pliensbachian (Jurassic) in the western
774 Tethys and adjacent areas. Palaeogeography, Palaeoclimatology, Palaeoecology 280, 64-
775 77.

776 Duarte, L.V., 1998. Clay minerals and geochemical evolution in the Toarcian-lower Aalenian
777 of the Lusitanian Basin (Portugal). Cuadernos de geología ibérica 24, 69-98.

778 Duarte, L.V., Comas-Rengifo, M.J., Silva, R.L., Paredes, R., Goy, A., 2014. Carbon isotope
779 stratigraphy and ammonite biochronostratigraphy across the Sinemurian-Pliensbachian
780 boundary in the western Iberian margin. Bulletin of Geosciences 89, 719-736.

781 Franceschi, M., Dal Corso, J., Posenato, R., Roghi, G., Masetti, D., Jenkyns, H.C., 2014. Early
782 Pliensbachian (Early Jurassic) C-isotope perturbation and the diffusion of the *Lithiotis*
783 Fauna: insights from the western Tethys. Palaeogeography, Palaeoclimatology,
784 Palaeoecology 410, 255-263.

785 Ghirardi J., Deconinck J.-F., Pellenard, P., Martinez, M., Bruneau, L., Amiotte-Suchet, P.,
786 Pucéat, E., 2014. Multi-proxy orbital chronology in the aftermath of the Aptian Oceanic
787 Anoxic Event 1a: Palaeoceanographic implications (Serre Chaitieu section, Vocontian
788 Basin, SE France). Newsletter on Stratigraphy 47, 247-262.

789 Godet, A., Bodin, S., Adatte, T., Föllmi, K.B., 2008. Platform-induced clay-mineral
790 fractionation along a northern Tethyan basin-platform transect: implications for the
791 interpretation of Early Cretaceous climate change (Late Hauterivian-Early Aptian).
792 Cretaceous Research 29, 830-847.

793 Gómez, J.J., Comas-Rengifo, M.J., Goy, A., 2016. Palaeoclimatic oscillations in the
794 Pliensbachian (Early Jurassic) of the Asturian Basin (Northern Spain). Climate of the Past
795 12, 1199-1214.

796 Gradstein, F.M., Ogg, J.G., Schmitz, M., Ogg, G., 2012. The Geologic Time Scale 2012.
797 Elsevier, Boston, 1176 p.

798 Guex, J., Pilet, S., Müntener, O., Bartolini, A., Spangenberg, J., Schoene, B., Sell, B.,
799 Schaltegger, U., 2016. Thermal erosion of cratonic lithosphere as a potential trigger for
800 mass-extinction. Scientific reports 6, doi: 10.1038/srep23168.

801 Guillocheau, F., Robin, C., Allemand, P., Bourquin, S., Brault, N., Dromart, G., Friedenberg,
802 R., Garcia, J.-P., Gaulier, J.-M., Gaumet, F., Grosdoy, B., Hanot, F., Le Strat, P.,
803 Mettraux, M., Nalpas, T., Prijac, C., Rigollet, C., Serrano, O., Grandjean, G., 2000. Meso-
804 Cenozoic geodynamic evolution of the Paris Basin: 3D stratigraphic constraints.
805 Geodinamica Acta 13, 189-246.

806 Hallam, A., Grose, J.A., Ruffell, A.H., 1991. Palaeoclimatic significance of changes in clay
807 mineralogy across the Jurassic-Cretaceous in England and France. Palaeogeography,
808 Palaeoclimatology, Palaeoecology 81, 173-187.

809 Hardenbol, J., Thierry, J., Farley, M.B., de Graciansky, P.-C., Vail, P.R., 1998. Mesozoic and
810 Cenozoic sequence chronostratigraphic framework of European basins. In: de
811 Graciansky, P.-C., Hardenbol, J., Jacquin, T., Vail, P. R. (Eds.), Mesozoic and Cenozoic

812 Sequence Stratigraphy of European basins. Special Publication, Society for Sedimentary
813 Geology 60, 3-13.

814 Hermoso, M., Le Callonnec, L., Minoletti, F., Renard, M., Hesselbo, S.P., 2009. Expression of
815 the Early Toarcian negative carbon-isotope excursion in separated carbonate
816 microfractions (Jurassic, Paris Basin). Earth and Planetary Science Letters 277, 194-203.

817 Hermoso, M., Minoletti, F., Rickaby, R.E.M., Hesselbo, S.P., Baudin, F., Jenkyns, H.C., 2012.
818 Dynamics of a stepped carbon-isotope excursion: Ultra high-resolution study of Early
819 Toarcian environmental change. Earth and Planetary Science Letters 319-320, 45-54.

820 Hermoso, M., Minoletti, F., Pellenard, P., 2013. Black shale deposition during Toarcian super-
821 greenhouse driven by sea level. Climate of the Past 9, 2703-2712.

822 Hermoso, M., Pellenard, P., 2014. Continental weathering and climatic changes inferred from
823 clay mineralogy and paired carbon isotopes across the early to the middle Toarcian in the
824 Paris Basin. Palaeogeography, Palaeoclimatology, Palaeoecology 399, 385-393.

825 Hesselbo, S.P., Jenkyns, H.C., 1995. A comparison of the Hettangian to Bajocian successions
826 of Dorset and Yorkshire. In: Taylor, P.D. (ed.) Field Geology of the British Jurassic.
827 Geological Society of London. p. 105-150.

828 Hesselbo, S.P., Gröcke, D.R., Jenkyns, H.C., Bjerrum, C.J., Farrimond, P., Morgans-Bell, H.S.,
829 Green, O.R., 2000. Massive dissociation of gas hydrate during a Jurassic oceanic anoxic
830 event. Nature 406, 392-395.

831 Hesselbo, S.P., Jenkyns, H.C., Duarte, L.V., Oliveira, L.C.V., 2007. Carbon-isotope record of
832 the Early Jurassic (Toarcian) Oceanic Anoxic Event from fossil wood and marine
833 carbonate (Lusitanian Basin, Portugal). Earth and Planetary Science Letters 253, 455-
834 470.

Hesselbo, S.P., Deconinck, J.-F., Huggett, J.M., Morgans-Bell, H.S., 2009. Late Jurassic palaeoclimatic change from clay mineralogy and gamma-ray spectrometry of the Kimmeridge Clay, Dorset, UK. Journal of the Geological Society 166, 1123-1133.

Hesselbo, S.P., Pieńkowski, G., 2011. Stepwise atmospheric carbon-isotope excursion during the Toarcian Oceanic Anoxic Event (Early Jurassic, Polish Basin). Earth and Planetary Science Letters 301, 365-372.

Hillier, S., Wilson, M.J., Merriman, R.J., 2006. Clay mineralogy of the Old Red Sandstone and Devonian sedimentary rocks of Wales, Scotland and England. Clay Minerals 41, 433-471.

Holtzapffel, T. (1985). Les minéraux argileux: préparation, analyse diffractométrique et détermination (Vol. 12). Société géologique du Nord, 135 p.

Hurst, A., 1985. The implications of clay mineralogy to palaeoclimate and provenance during the Jurassic in NE Scotland. Scottish Journal of Geology 21, 143-160.

Izumi, K., Miyaji, T., Tanabe, K., 2012. Early Toarcian (Early Jurassic) oceanic anoxic event recorded in the shelf deposits in the northwestern Panthalassa: Evidence from the Nishinakayama Formation in the Toyora area, west Japan. Palaeogeography, Palaeoclimatology, Palaeoecology 315-316, 100-108.

Jacquin, T., de Graciansky, P.-C., 1998. Major transgressive/regressive cycles: the stratigraphic signature of European basin development. Mesozoic and Cenozoic Sequence Stratigraphy of European basins, SEPM special publication 60, 15-29.

Jeans, C.V., 2006. Clay mineralogy of the Jurassic strata of the British Isles. Clay Minerals 41, 187-307.

857 Jenkyns, H.C., 1988. The early Toarcian (Jurassic) anoxic event: stratigraphic, sedimentary,
858 and geochemical evidence. American Journal of Science 288, 101–151.

859 Jenkyns, H.C., Jones, C.E., Gröcke, D.R., Hesselbo, S.P., Parkinson, D.N., 2002.
860 Chemostratigraphy of the Jurassic System: applications, limitations and implications for
861 palaeoceanography. Journal of the Geological Society 159, 351-378.

862 Jenkyns, H.C., 2010. Geochemistry of oceanic anoxic events. Geochemistry, Geophysics,
863 Geosystems 11, Q03004, doi: 10.1029/2009GC002788.

864 Jones, C.E., Jenkyns, H.C., Hesselbo, S.P., 1994. Strontium isotopes in Early Jurassic seawater.
865 Geochimica et Cosmochimica Acta 58, 1285-1301.

866 Jones, C.E., Jenkyns, H.C., 2001. Seawater strontium isotopes, Oceanic Anoxic Events, and
867 sea-floor hydrothermal activity in the Jurassic and Cretaceous. American Journal of
868 Science 301, 112-149.

869 Jourdan, F., Féraud, G., Bertrand, H., Watkeys, M.K., Renne, P.R., 2008. The $^{40}Ar/^{39}Ar$ ages
870 of the sill complex of the Karoo large igneous province: Implications for the
871 Pliensbachian-Toarcian climate change. Geochemistry, Geophysics, Geosystems 9,
872 Q06009, doi:10.1029/2008GC001994.

873 Kemp, D.B., Coe, A.L., Cohen, A.S., Schwark, L., 2005. Astronomical pacing of methane
874 release in the Early Jurassic period. Nature 437, 396-399.

875 Korte, C., Hesselbo, S.P., 2011. Shallow marine carbon and oxygen isotope and elemental
876 records indicate icehouse-greenhouse cycles during the Early Jurassic. Paleoceanography
877 26, PA4219, doi:10.1029/2011PA002160.

878 Krencker, F.N., Bodin, S., Hoffmann, R., Suan, G., Mattioli, E., Kabiri, L., Föllmi, K.B.,
879 Immenhauser, A., 2014. The middle Toarcian cold snap: Trigger of mass extinction and
880 carbonate factory demise. Global and Planetary Change 117, 64-78.

881 Lanson, B., Beaufort, D., Berger, G., Bauer, A., Cassagnabère, A., Meunier, A., 2002.
882 Authigenic kaolin and illitic minerals during burial diagenesis of sandstones: a review.
883 Clay Minerals 37, 1-22.

884 Lanson, B., Sakharov, B. A., Claret, F., Drits, V.A., 2009. Diagenetic smectite-to-illite
885 transition in clay-rich sediments: a reappraisal of X-ray diffraction results using the multi-
886 specimen method. American Journal of Science 309, 476-516.

887 Lavastre, V., Ader, M., Buschaert, S., Petit, E., Javoy, M., 2011. Water circulation control on
888 carbonate-$\delta^{18}O$ records in a low permeability clay formation and surrounding limestones:
889 The Upper Dogger–Oxfordian sequence from the eastern Paris basin, France. Applied
890 Geochemistry 26, 818-827.

891 Léonide, P., Floquet, M., Durlet, C., Baudin, F., Pittet, B., Lécuyer, C., 2012. Drowning of the
892 carbonate platform as a precursor stage of the Early Toarcian global anoxic event
893 (Southern Provence sub-Basin, South-east France). Sedimentology 59, 156-184.

894 Lézin, C., Andreu, B., Pellenard, P., Bouchez, J.-L., Emmanuel, L., Fauré, P., Landrein, P.,
895 2013. Geochemical disturbance and paleoenvironmental changes during the Early
896 Toarcian in NW Europe. Chemical Geology 341, 1-15.

897 Little, C.T.S., Benton, M.J., 1995. Early Jurassic mass extinction: A global long-term event.
898 Geology 23, 495-498.

899 Lorenz, J., Lefavrais, A., Depeche, F., Leclerc, V., Marchand, D., Roy, B., Taugourdeau , J.,
900 Reyre, Y., 1987. Le Jurassique. In: Lorenz, C. (Ed.), Forage scientifique de Sancerre-

Couy (Cher). In: Documents du Bureau de Recherches Géologiques et Minières, vol. 136. Bureau de Recherches Géologiques et Minières, pp.19-26.

Marron, J.S., Chaudhuri, P., 1998. When is a feature really there? The SiZer approach. In: Firooz, A., (Eds.). Automatic target recognition VII: Photooptic and Industrial Engineering Proceedings 3371, 306-312.

Marshall, J.D., 1992. Climatic and oceanographic isotopic signals from the carbonate rock record and their preservation. Geological magazine 129, 143-160.

Martinez, M., Dera, G., 2015. Orbital pacing of carbon fluxes by a ~9-My eccentricity cycle during the Mesozoic. Proceedings of the National Academy of Sciences 112, 12604-12609.

Merriman, R.J., Frey, M., 1999. Patterns of very low-grade metamorphism in metapelitic rocks. In: Frey, M., Robinson, D. (Eds.). Low-Grade Metamorphism. Blackwell Science Ltd, pp. 61-107.

Moiroud, M., Martinez, M., Deconinck, J.-F., Monna, F., Pellenard, P., Riquier, L., Company, M., 2012. High-resolution clay mineralogy as a proxy for orbital tuning: Example of the Hauterivian–Barremian transition in the Betic Cordillera (SE Spain). Sedimentary Geology 282, 336-346.

Moore, D.M., Reynolds, R.C., 1997. X-Ray Diffraction and the Identification and Analysis of 679 Clay Minerals. Oxford University Press, New York, 400 p.

Moreau, M.-G., Bucher, H., Bodergat, A.-M., Guex, J., 2002. Pliensbachian magnetostratigraphy: new data from Paris Basin (France). Earth and Planetary Science Letters 203, 755-767.

923 Mørk, M.B.E., Vigron, J.O., Smelror, M., Fjerdingstad, V., Bøe, R. 2003. Mesozoic mudstone
924 compositions and the role of kaolinite weathering - a view from shallow cores in the
925 Norwegian Sea (Møre to Troms). Norwegian Journal of Geology 83, 61-78.

926 Neumeister, S., Gratzer, R., Algeo, T.J., Bechtel, A., Gawlick, H.-J., Newton, R.J.,
927 Sachsenhofer, R.F., 2015. Oceanic response to Pliensbachian and Toarcian magmatic
928 events: Implications from an organic-rich basinal succession in the NW Tethys. Global
929 and Planetary Change 126, 62-83.

930 Oliveira, L.C.V., Rodrigues, R., Duarte, L.V., Brasil Lemos, V., 2006. Avaliação do potencial
931 gerador de petróleo e interpretação paleoambiental com base em biomarcadores e
932 isótopos estáveis de carbono da seção Pliensbaquiano–Toarciano inferior (Jurássico
933 Inferior) da região de Peniche (Bacia Lusitânica, Portugal). Boletim de Geociências da
934 Petrobras 14, 207-234.

935 Pálfy, J., Smith, P.L., 2000. Synchrony between Early Jurassic extinction, oceanic anoxic event,
936 and the Karoo-Ferrar flood basalt volcanism. Geology 28, 747-750.

937 Paquet, H., Clauer N., 1997. Soils and Sediments, Mineralogy and Geochemistry. Springer
938 Verlag, Berlin-Heidelberg, 369 p.

939 Pellenard, P., Deconinck, J.-F., 2006. Mineralogical variability of Callovo-Oxfordian clays
940 from the Paris Basin and the Subalpine Basin. Comptes Rendus Geoscience 338, 854-
941 866.

942 Pellenard, P., Tramoy, R., Pucéat, E., Huret, E., Martinez, M., Bruneau, L., Thierry, J., 2014.
943 Carbon cycle and sea-water palaeotemperature evolution at the Middle-Late Jurassic
944 transition, eastern Paris Basin (France). Marine and Petroleum Geology 53, 30-43.

945 Peti, L., Thibault, N., Clémence, M.-E., Korte, C., Dommergues, J.-L., Bougeault, C.,
946 Pellenard, P., Ullmann, C.V. (in press). Sinemurian-Pliensbachian calcareous nannofossil
947 biostratigraphy and organic carbon isotope stratigraphy in the Paris Basin: calibration to
948 the ammonite biozonation of NW Europe.

949 Petschick, R., 2000. MacDiff 4.2.2. Available online:
950 http://servermac.geologie.unfrankfurt.de/Rainer.html

951 Price, G.D., 1999. The evidence and implications of polar ice during the Mesozoic. Earth-
952 Science Reviews 48, 183-210.

953 Price, G.D., Baker, S.J., VanDeVelde, J., Clémence, M.E. 2016. High-resolution carbon cycle
954 and seawater temperature evolution during the Early Jurassic (Sinemurian-Early
955 Pliensbachian). Geochemistry, Geophysics, Geosystems 17, doi:
956 10.1002/2016GC006541.

957 Raucsik, B., Varga, A., 2008. Climato-environmental controls on clay mineralogy of the
958 Hettangian–Bajocian successions of the Mecsek Mountains, Hungary: An evidence for
959 extreme continental weathering during the early Toarcian oceanic anoxic event.
960 Palaeogeography, Palaeoclimatology, Palaeoecology 265, 1-13.

961 Rees, P.M., Ziegler, A.M., Valdes, P.J., 2000. Jurassic phytogeography and climates: new data
962 and model comparisons. In: Huber, B.T., Macleod, K.G., Wing, S.L. (Eds.), Warm
963 climates in Earth history. Cambridge University Press, pp. 297-318.

964 Robert, C., Kennett, J.P., 1994. Antarctic subtropical humid episode at the Paleocene-Eocene
965 boundary: Clay-mineral evidence. Geology 22, 211-214.

966 Rosales, I., Quesada, S., Robles, S., 2004. Paleotemperature variations of Early Jurassic
967 seawater recorded in geochemical trends of belemnites from the Basque-Cantabrian

968 basin, northern Spain. Palaeogeography, Palaeoclimatology, Palaeoecology 203, 253-
969 275.

970 Rosales, I., Quesada, S., Robles, S., 2006. Geochemical arguments for identifying second-order
971 sea-level changes in hemipelagic carbonate ramp deposits. Terra Nova 18, 233-240.

972 Ruffell, A., McKinley, J.M., Worden, R.H., 2002. Comparison of clay mineral stratigraphy to
973 other proxy palaeoclimate indicators in the Mesozoic of NW Europe. Philosophical
974 Transactions of the Royal Society A 360, 675-693.

975 Ruhl, M., Hesselbo, S.P., Hinnov, L., Jenkyns, H.C., Xu, W., Riding, J.B., Storm, M., Minisini,
976 D., Ullmann, C.V., Leng, M.J., 2016. Astronomical constraints on the duration of the
977 Early Jurassic Pliensbachian Stage and global climatic fluctuations. Earth and Planetary
978 Science Letters 455, 149-165.

979 Schaltegger, U., Guex, J., Bartolini, A., Schoene, B., Ovtcharova, M., 2008. Precise U-Pb age
980 constraints for end-Triassic mass extinction, its correlation to volcanism and Hettangian
981 post-extinction recovery. Earth and Planetary Science Letters 267, 266-275.

982 Schnyder J., Baudin F., Deconinck J.-F., Durlet C., Jan du Chene R., Lathuilière B., 2000.
983 Stratigraphie et analyse sédimentologique du passage Oxfordien/Kimméridgien dans le
984 Boulonnais. Géologie de la France 4, 21-37.

985 Schnyder, J., Ruffell, A., Baudin, F., Deconinck, J.-F., 2006. Conjunctive use of clay
986 mineralogy and spectral gamma-ray logs in defining late Jurassic-early Cretaceous
987 palaeoclimate change (Dorset, U.K.). Palaeogeography, Palaeoclimatology,
988 Palaeoecology 229, 303-320.

989 Schouten, S., van Kaam-Peters, H.M.E., Rijpstra, W.I.C., Schoell, M., Sinnighe Damste, J.S.,
990 2000. Effects of an oceanic anoxic event on the stable carbon isotopic composition of
991 early Toarcian carbon. American Journal of Science 300, 1-22.

992 Shaw, H.F., 2006. Clay mineralogy of Carboniferous sandstone reservoirs, onshore and
993 offshore UK. Clay Minerals 41, 417-432.

994 Silva, R.L., Duarte, L.V., Comas-Rengifo, M.J., Mendonça Filho, J.G., Azerêdo A.C., 2011.
995 Update of the carbon and oxygen isotopic records of the Early-Late Pliensbachian (Early
996 Jurassic, ~187 Ma): Insights from the organic-rich hemipelagic series of the Lusitanian
997 Basin (Portugal). Chemical Geology 283, 177-184.

998 Silva, R.L., Duarte, L.V., 2015. Organic matter production and preservation in the Lusitanian
999 Basin (Portugal) and Pliensbachian climatic hot snaps. Global and Planetary Change 131,
1000 24-34.

1001 Środoń, J., Clauer, N., Huff, W., Dudek, T., Banaś, M., 2009. K-Ar dating of the Lower
1002 Palaeozoic K-bentonites from the Baltic Basin and the Baltic Shield: implications for the
1003 role of temperature and time in the illitization of smectite. Clay minerals 44, 361-387.

1004 Steinthorsdottir, M., Vajda, V., 2015. Early Jurassic (late Pliensbachian) CO_2 concentrations
1005 based on stomatal analysis of fossil conifer leaves from eastern Australia. Gondwana
1006 Research 27, 932-939.

1007 Suan, G., Mattioli, E., Pittet, B., Lécuyer, C., Suchéras-Marx, B., Duarte, L.V., Philippe, M.,
1008 Reggiani, L., Martineau, F., 2010. Secular environmental precursors to Early Toarcian
1009 (Jurassic) extreme climate changes. Earth and Planetary Science Letters 290, 448-458.

1010 Suan, G., Nikitenko, B.L., Rogov, M.A., Baudin, F., Spangenberg, J.E., Knyazev, V.G.,
1011 Glinskikh, L.A., Goryacheva, A.A., Adatte, T., Riding, J.B., Föllmi, K.B., Pittet, B.,

1012 Mattioli, E., Lécuyer, C., 2011. Polar record of Early Jurassic massive carbon injection.
1013 Earth and Planetary Science Letters 312, 102-113.

1014 Thierry, J. et al. (40 co-authors), 2000. Late Sinemurian. In: Dercourt, J., Gaetani, M.,
1015 Vrielynck, B., Barrier, E., Biju-Duval, B., Brunet, M.-F., Cadet, J.P., Crasquin, S.,
1016 Sandulescu, M. (Eds.), Atlas Peri-Tethys Paleogeographical Maps, vol. I–
1017 XX.CCGM/CGMW, Paris, pp. 49-59.

1018 Thiry, M., 2000. Palaeoclimatic interpretation of clay minerals in marine deposits: an outlook
1019 from the continental origin. Earth-Science Reviews 49, 201-221.

1020 Van de Schootbrugge, B., Bailey, T.R., Rosenthal, Y., Katz, M.E., Wright, J.D., Miller, K.G.,
1021 Feist-Burkhardt, S., Falkowski, P.G., 2005. Early Jurassic climate change and the
1022 radiation of organic-walled phytoplankton in the Tethys Ocean. Paleobiology 31, 73-97.

1023 Vanderaveroet, P., Averbuch, O., Deconinck, J.-F., Chamley, H., 1999. A record of
1024 glacial/interglacial alternations in Pleistocene sediments off New Jersey expressed by
1025 clay mineral, grain-size and magnetic susceptibility data. Marine Geology 159, 79-92.

1026 Vercoutere, C., Van den Haute, P., 1993. Post-Palaeozoic cooling and uplift of the Brabant
1027 Massif as revealed by apatite fission track analysis. Geological Magazine 130, 639-646.

1028 Wignall, P.B., 2001. Large igneous provinces and mass extinctions. Earth-Science Reviews 53,
1029 1-33.

1030 Wignall, P.B., Newton, R.J., Little, C.T., 2005. The timing of paleoenvironmental change and
1031 cause-and-effect relationships during the Early Jurassic mass extinction in Europe.
1032 American Journal of Science 305, 1014-1032.

1033 Worden, R.H., Morad, S., 2003. Clay minerals in sandstones: controls on formation,
1034 distribution and evolution. Clay mineral cements in sandstones, 1-41.

1035 Yang, Z., Moreau, M.-G., Bucher, H., Dommergues, J.-L., Trouiller, A., 1996. Hettangian and
1036 Sinemurian magnetostratigraphy from Paris Basin. Journal of Geophysical Research 101,
1037 8025-8042.

1038 Figure captions:

1039 Figure 1. Position of studied boreholes and outcrops on the Early Jurassic palaeomap (modified
1040 from Blakey's palaeomap: https://deeptimemaps.com/ and Thierry et al., 2000). Abbreviations:
1041 SM=Scottish Massif; IrM=Irish Massif; CM= Cornubian Massif; WH=Welsh High; LBM=
1042 London-Brabant Massif; RM=Rhenish Massif; BM=Bohemian Massif; MC=Massif Central;
1043 AM=Armorican Massif; IbM=Iberian Massif.

1044 Figure 2. Detailed lithology, sampling and ammonite biostratigraphy of the Montcornet
1045 borehole.

1046 Figure 3. Biostratigraphy, lithology, sequence stratigraphy, clay mineralogy, K/I
1047 (kaolinite/illite) ratio and associated SiZer map, $\delta^{13}C$ from organic matter, in the Sancerre
1048 borehole (Southern Paris Basin). Smoothed curves with their 95% confidence interval have
1049 been calculated using Kernel regressions for K/I ratio and $\delta^{13}C_{org}$. Ammonite zone and subzone
1050 abbreviations: Gib.=Gibbosus; Raricos.=Raricostatum; Sub.=Subnodosus;
1051 Tenuicos.=Tenuicostatum. Grey cases correspond to uncertainties in the biostratigraphic
1052 framework.

1053 Figure 4. Biostratigraphy, lithology, sequence stratigraphy, clay mineralogy, K/I
1054 (kaolinite/illite) ratio and associated SiZer map, $\delta^{13}C$ from bulk carbonate in the Montcornet
1055 borehole (Northern Paris Basin). Smoothed curves with their 95% confidence interval have
1056 been calculated using Kernel regressions for K/I ratio and $\delta^{13}C_{carb}$. Ammonite zone and subzone
1057 abbreviations: C.=Capricornus; Gib.=Gibbosus; J.=Jamesoni; Mac.=Macdonelli;
1058 M.=Maculatum; P.=Polymorphus; Rar.=Raricostatum; Sub.=Subnodosus. Grey cases
1059 correspond to uncertainties in the biostratigraphic framework. The legend is the same as fig. 3.

1060 Figure 5. Scanning Electron Microscope from samples of Montcornet. A-B) views of a
1061 limestone bed sample (772.75 m), displaying calcite mixed with detrital clays; C) zoom of the

same sample (772.75 m) showing typical authigenic vermicular kaolinite formed inside porosity; D) view of clayey sample (812.9 m) showing common detrital clay fabric with some framboidal pyrites.

Figure 6. Correlation between Sancerre and Montcornet boreholes (Paris Basin) and two additional outcrops from Charmouth (Wessex Basin) and Corbigny (Paris Basin). Red intervals indicate an increase in the K/I ratio while the blue intervals indicate a decrease in the K/I ratio. Yellow intervals correspond to the main $\delta^{13}C$ negative excursions identified in the two boreholes (SPBE: Sinemurian Pliensbachian Boundary Event; T-OAE: Toarcian Oceanic Anoxic Event). Ammonite zone and subzone abbreviations: B.=Brevispina; C.= Capricornus; F.=Figulinum; Gib.=Gibbosus; Ib.=Ibex; J.=Jamesoni; L.=Luridum; Mac.=Macdonelli; M.=Masseanum; P.=Polymorphus; M.=Maculatum; Rar./Raricos=Raricostatum; Sub.= Subnodosus; T.=Taylori; V.=Valdani. Grey cases correspond to uncertainties in the biostratigraphic framework.

Figure 7. Palaeomaps and schematic cross-sections for clay minerals sourcing in: A) sea-level lowstand configuration; B) sea-level highstand configuration. Abbreviations of Massifs and discussed sections: AM=Armorican Massif; BM=Bohemian Massif; Co=Corbigny; CB=Cleveland Basin; Ch=Charmouth; CM=Cornubian Massif; LBM=London-Brabant Massif; IbM=Iberian Massif; IrM=Irish Massif; Mo=Montcornet; MC=Massif Central; PB=Paris Basin; Sa=Sancerre; RM=Rhenish Massif; SM=Scottish Massif; WH=Welsh High. Clay mineral abbreviations: C=chlorite; I=illite; K=kaolinite; S=smectite. Palaeocurrents are based on Bjerrum et al., 2001 and Dera et al., 2015.

Figure 8. Summary of clay mineral data, geochemical data, and organic matter accumulations from the end Sinemurian to the early Toarcian, reported against numerical ages, biostratigraphic framework based on ammonites and sequence stratigraphy of the Tethyan domain (Jacquin et

1086 al., 1998; Gradstein et al., 2012): Smectite events (this study); $\delta^{18}O$ from belemnites (dataset
1087 from Martinez and Dera, 2015) with red intervals corresponding to warm periods and blue
1088 intervals to cold periods; runoff based on the K/I ratio (this study), with position of small K/I
1089 increase (1, 2, 3) and major K/I increase (A) and decrease (B); $\delta^{13}C$ from organic matter
1090 (Hesselbo et al., 2000, 2007; van de Schootbrugge et al., 2005; Suan et al., 2010; Korte and
1091 Hesselbo, 2011), $\delta^{13}C$ from bulk carbonates (Oliveira et al., 2006; Silva et al., 2011; Duarte et
1092 al., 2014; this study) and $\delta^{13}C$ from belemnite data (Martinez and Dera, 2015), with yellow
1093 intervals corresponding to main negative carbon excursions; black shale occurrence (black
1094 point), the point size indicates their record extent (Rosales et al., 2004; Oliveira et al, 2006;
1095 Silva et al., 2011; Armendáriz et al., 2012; Boussaha et al., 2014; Duarte et al., 2014); $^{87}Sr/^{86}Sr$
1096 curve (Jones et al., 1994) and εNd curve (Dera et al., 2009b).

1097

1098 Supplementary material:

1099 Table 1: Sampled and identified ammonites in the Montcornet borehole

1100 Table 2: Clay mineral proportion in the Montcornet borehole. (IS R0: R0 type illite smectite
1101 mixed-layer; C: chlorite; IS R1: R1 type illite smectite mixed-layer; I: illite; K: kaolinite; K/I:
1102 kaolinite/illite ratio.

1103 Table 3: Clay mineral proportion in the Montcornet borehole. (IS R0: R0 type illite smectite
1104 mixed-layer; C: chlorite; IS R1: R1 type illite smectite mixed-layer; I: illite; K: kaolinite; K/I:
1105 kaolinite/illite ratio.

1106 Table 4: $\delta^{13}C$ and $\delta^{18}O$ form bulk carbonate values (expressed in ‰) in the Montcornet
1107 borehole.

1108 Fig. 1: Biochronology from North-Western Europe and distribution of ammonites fauna in the
1109 Montcornet borehole.

1110

1111 Fig. 2: $\delta^{13}C$ and $\delta^{18}O$ values from bulk carbonate in the Montcornet borehole (Northern Paris

1112 Basin).

1113

1114

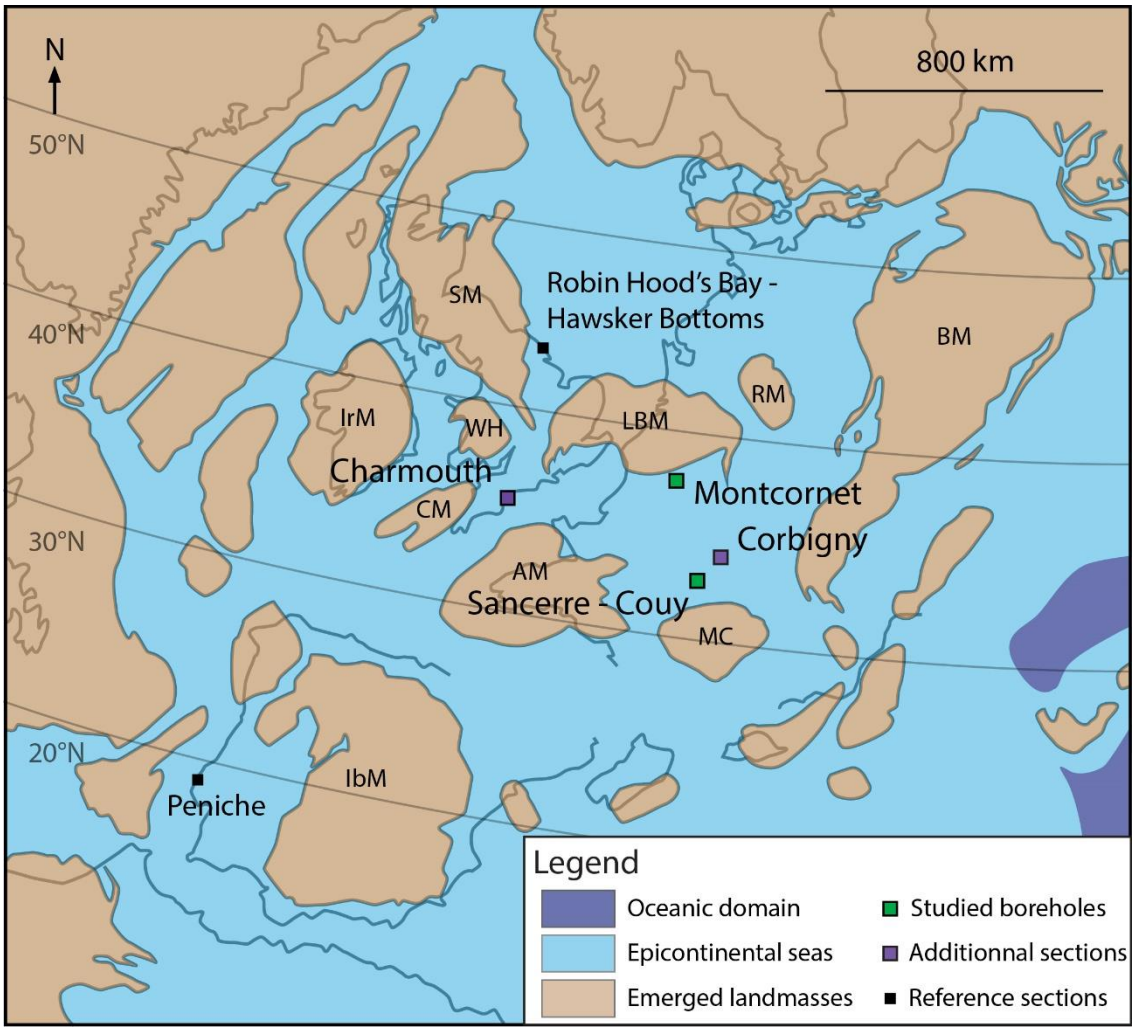
N
800 km
50°N
40°N
30°N
20°N
SM
Robin Hood's Bay -
Hawsker Bottoms
BM
RM
IrM
WH
LBM
Charmouth
CM
Montcornet
Corbigny
AM
Sancerre - Couy
MC
IbM
Peniche
Legend
Oceanic domain
Epicontinental seas
Emerged landmasses
Studied boreholes
Additionnal sections
Reference sections

Fig 1

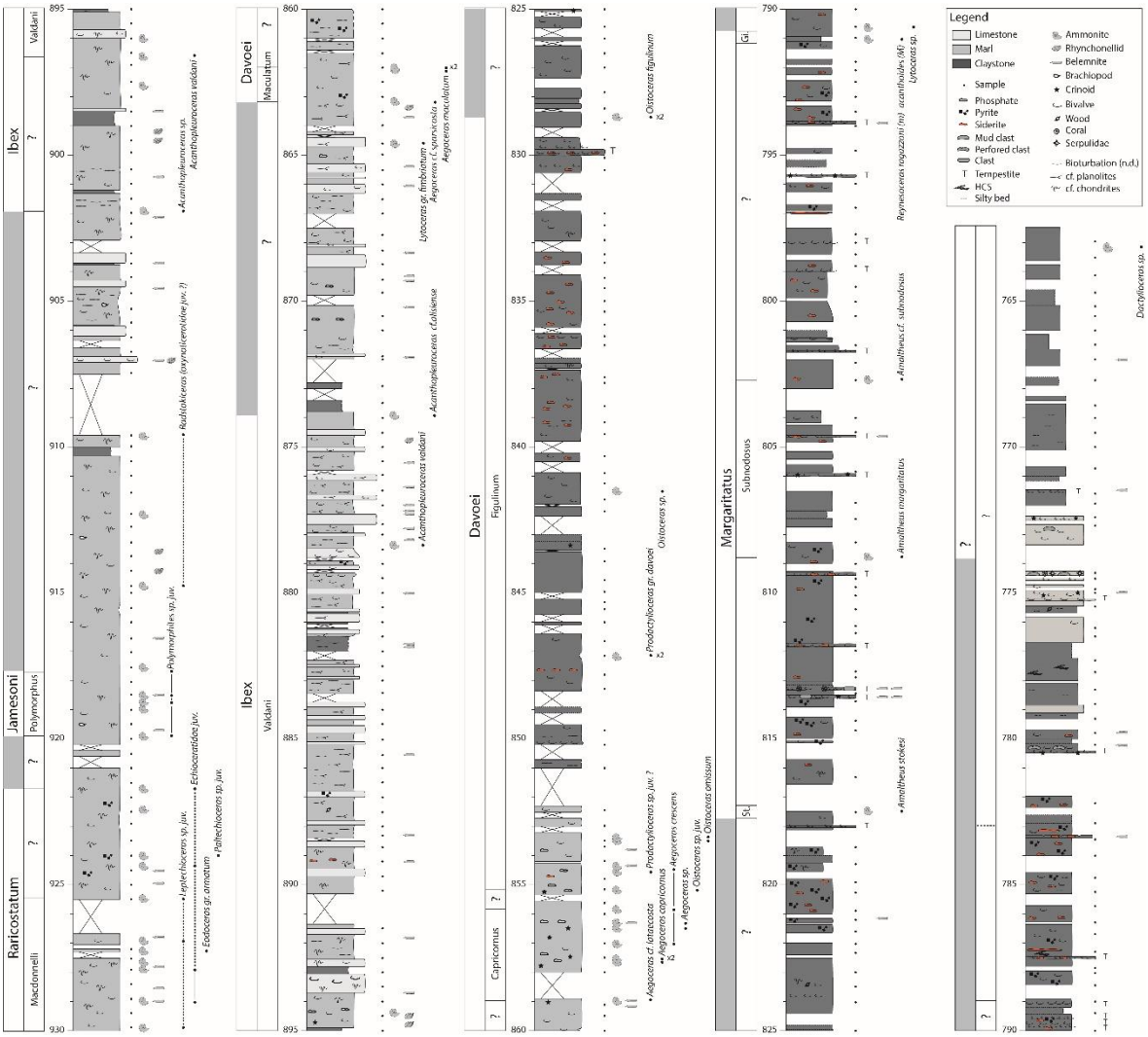
Ibex
Jamesoni
Raricostatum
Macdonnelli
Polymorphus
Valdani
Davoei
Maculatum
Ibex
Valdani
Davoei
Figulinum
Capricornus
Margaritatus
Subnodosus
Legend
Limestone
Marl
Claystone
Sample
Phosphate
Pyrite
Siderite
Mud clast
Perfored clast
Clast
Tempestite
HCS
Silty bed
Ammonite
Rhynchonellid
Belemnite
Brachiopod
Crinoid
Bivalve
Wood
Coral
Serpulidae
Bioturbation (n.d.)
cf. planolites
cf. chondrites

Fig 2

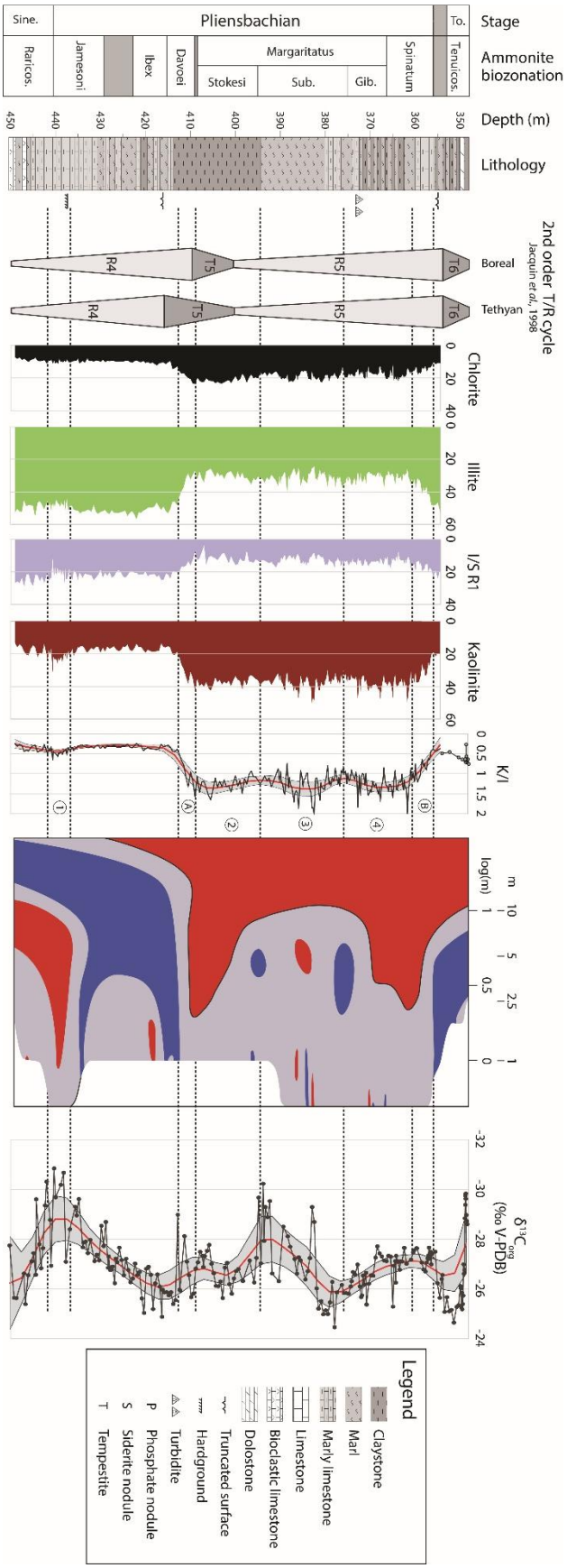
Sine.
Pliensbachian
To.
Stage
Raricos.
Jamesoni
Ibex
Davoei
Margaritatus
Spinatum
Tenuicos.
Ammonite biozonation
Stokesi
Sub.
Gib.
Depth (m)
Lithology
2nd order T/R cycle
Jacquin et al., 1998
Boreal
Tethyan
R4
T5
R5
T6
Chlorite
Illite
I/S R1
Kaolinite
K/I
log(m)
$\delta^{13}C_{org}$ (‰ V-PDB)
Legend
Claystone
Marl
Marly limestone
Limestone
Bioclastic limestone
Dolostone
Truncated surface
Hardground
Turbidite
Phosphate nodule
Siderite nodule
Tempestite

Fig 3

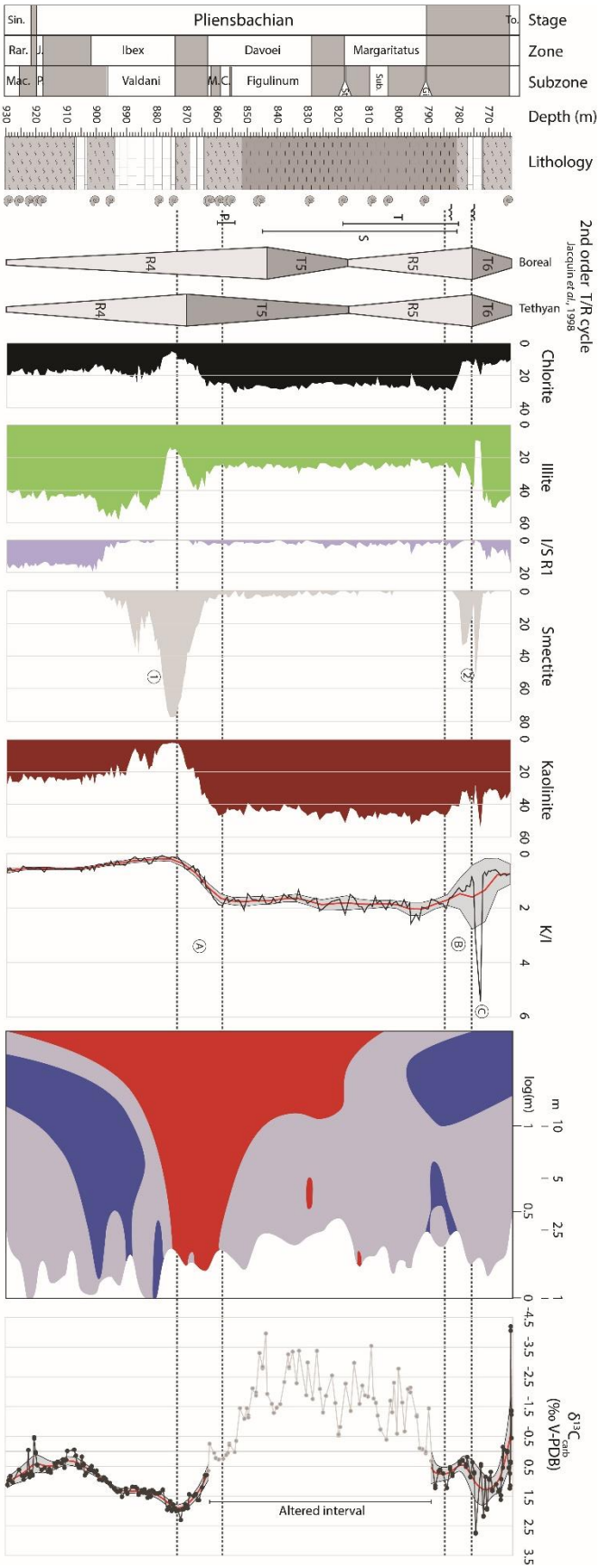
Sin.
Pliensbachian
To.
Stage
Rar.
Ibex
Davoei
Margaritatus
Zone
Mac.
Valdani
M.C.
Figulinum
Sub.
Subzone
Depth (m)
Lithology
2nd order T/R cycle
Jacquin et al., 1998
Boreal
Tethyan
R4
T5
R5
T6
Chlorite
Illite
I/S R1
Smectite
Kaolinite
K/I
log(m)
m
δ13Ccarb (‰ V-PDB)
Altered interval

Fig 4

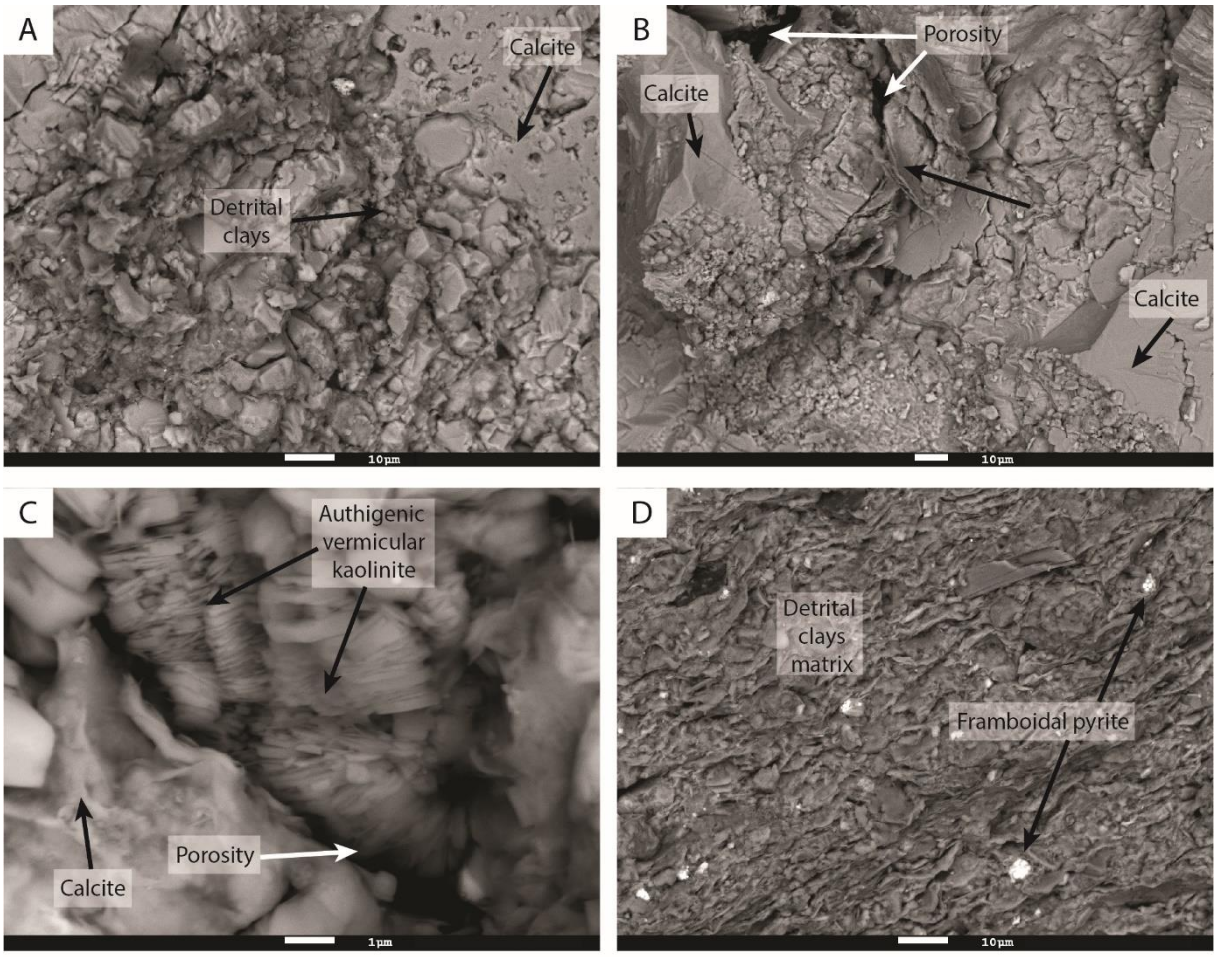
A
Calcite
Detrital clays
10µm
B
Porosity
Calcite
Calcite
10µm
C
Authigenic vermicular kaolinite
Porosity
Calcite
1µm
D
Detrital clays matrix
Framboidal pyrite
10µm

Fig 5

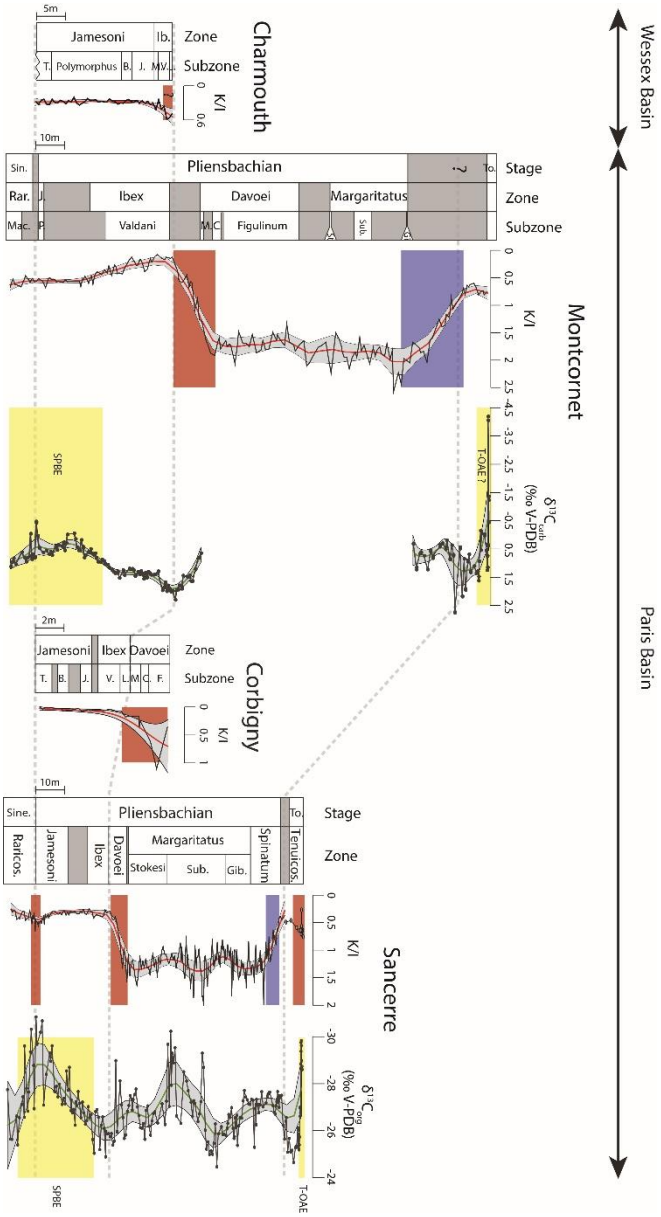
Wessex Basin
Paris Basin
Charmouth
Montcornet
Corbigny
Sancerre
Zone
Subzone
Stage
Jamesoni
Polymorphus
Pliensbachian
Ibex
Davoei
Margaritatus
Valdani
Figulinum
Sinemurian
Raricostatum
Spinatum
Stokesi
Tenuicostatum
SPBE
T-OAE
T-OAE?
K/I
5m
10m
2m

Fig 6

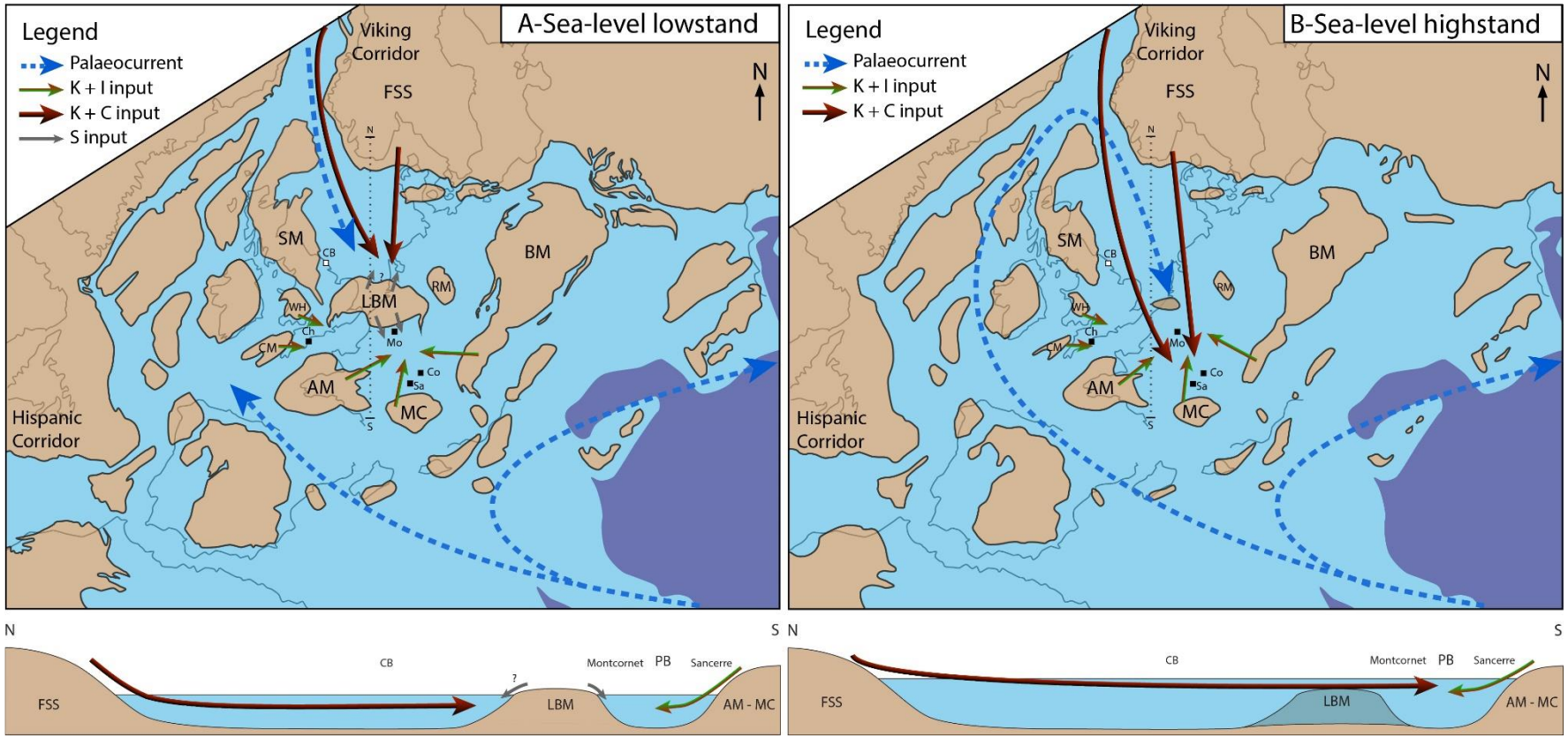
A-Sea-level lowstand
B-Sea-level highstand
Legend
Palaeocurrent
K + I input
K + C input
S input
Viking Corridor
FSS
N
SM
CB
BM
RM
LBM
WH
Ch
CM
Mo
Co
Sa
AM
MC
Hispanic Corridor
S
CB
Montcornet
PB
Sancerre
AM - MC

Fig 7

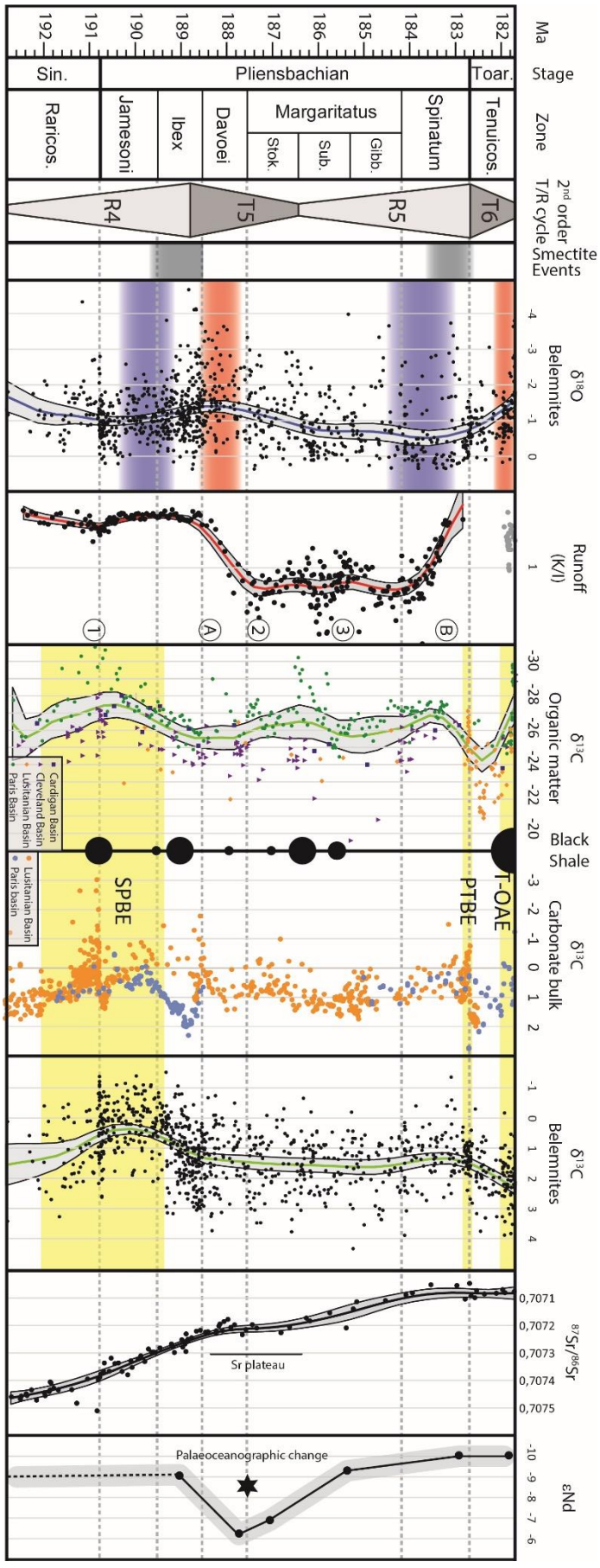
Ma
Stage
Zone
2nd order T/R cycle
Smectite Events
δ18O Belemnites
Runoff (K/I)
δ13C Organic matter
Black Shale
δ13C Carbonate bulk
δ13C Belemnites
87Sr/86Sr
εNd
Sin.
Pliensbachian
Toar.
Raricos.
Jamesoni
Ibex
Davoei
Margaritatus
Stok.
Sub.
Gibb.
Spinatum
Tenuicos.
R4
T5
R5
T6
Cardigan Basin
Cleveland Basin
Lusitanian Basin
Paris Basin
SPBE
PTBE
T-OAE
Sr plateau
Palaeoceanographic change

Fig 8